Calhoun: The NPS Institutional Archive

DSpace Repository

Theses and Dissertations | 1. Thesis and Dissertation Collection, all items

2013-06

Material characterization of high-voltage lithium-ion battery models for crashworthiness analysis

Meier, Joseph D.

Monterey California. Naval Postgraduate School

http://hdl.handle.net/10945/40234

This publication is a work of the U.S. Government as defined in Title 17, United States Code, Section 101. Copyright protection is not available for this work in the United States.

Downloaded from NPS Archive: Calhoun

http://www.nps.edu/library

Calhoun is the Naval Postgraduate School's public access digital repository for research materials and institutional publications created by the NPS community. Calhoun is named for Professor of Mathematics Guy K. Calhoun, NPS's first appointed -- and published -- scholarly author.

Dudley Knox Library / Naval Postgraduate School
411 Dyer Road / 1 University Circle
Monterey, California USA 93943

Material Characterization of High-Voltage Lithium-Ion Battery Models for Crashworthiness Analysis

By

Joseph D. Meier

Bachelor of Science in Mechanical Engineering
Auburn University Alabama, 2001

SUBMITTED TO THE DEPARTMENT OF MECHANICAL ENGINEERING
IN PARTIAL FULFILLMENT OF THE REQUIREMENTS FOR THE DEGREES OF

NAVAL ENGINEER

AND

MASTER OF SCIENCE IN MECHANICAL ENGINEERING

AT THE
MASSACHUSETTS INSTITUTE OF TECHNOLOGY
JUNE 2013

© 2013 Joseph D. Meier. All rights reserved.

The author hereby grants to MIT permission to reproduce and to distribute publicly paper and electronic copies of this thesis document in whole or in part in any medium now known or hereafter created.

Signature of Author [redacted]
Joseph D. Meier
Department of Mechanical Engineering
May 6, 2013

Certified by [redacted]
Tomasz Wierzbicki
Professor of Mechanical Engineering
Thesis Supervisor

Accepted by [redacted]
David Hardt
Chairman, Committee for Graduate Students
Department of Mechanical Engineering

(This Page Intentionally Blank)

Material Characterization of High-Voltage Lithium-Ion Battery Models for Crashworthiness Analysis

By
Joseph D. Meier

Submitted to the Department of Mechanical Engineering
on May 6, 2013 in Partial Fulfillment of the Requirements for the Degrees of
Naval Engineer and Master of Science in Mechanical Engineering

Abstract

A three-phased study of the material properties and post-impact behavior of prismatic pouch lithium-ion battery cells was conducted to refine computational finite element models and explore the mechanisms of thermal runaway caused by internal short circuit.

In phase one, medium and large sized cells at low state of charge (SOC) were impacted or compressed while measuring punch load, displacement, cell voltage, and surface temperature until an internal short circuit was detected, followed by a rise in surface temperature. Results were used to either refine the constitutive cell properties or validate finite element models.

In phase two, an exploratory study into the behavior of lithium-ion prismatic pouch battery cells following surface impacts with hemispherical and conical punches (abuse testing) was conducted for the purpose of observing pouch behavior and adequacy of parameter measurement methods. Cells were impacted by steel punches to loads as high as 500 kN while recording punch load, displacement, and pouch surface temperatures, as well as normal and high-speed video footage. Comparisons of load, surface temperature, and thermal runaway for various states of charge and punch types are presented.

In the third and final phase of the study, material characterization of cell components was conducted to further refine computational models and draw conclusions regarding the interactions between impacted cell layers and the physical cause of internal short circuits. Results of uniaxial tension tests for coated and uncoated anode and cathode layers, as well as separator layers are presented, as well as conclusions about the use of digital image correlation (DIC) software in such studies.

Much of the data generated was used to further refine and validate prismatic pouch lithium-ion battery cell computational models developed by the MIT Impact and Crashworthiness Laboratory. Physical tests conducted in phase one of this study were compared to model simulations, which showed that the models make close approximations for material displacement, and are good predictors of internal short circuit.

Thesis Supervisor: Tomasz Wierzbicki
Title: Professor of Structural Mechanics

(This Page Intentionally Blank)

Table of Contents

Abstract 3

Table of Contents 5

List of Figures 7

List of Tables 9

List of Acronyms and Abbreviations 9

Acknowledgements 11

1.0 Introduction 13

1.1 Motivation for Research 13

1.2 Related Research (2010-2012) 14

Representative Volume Element (RVE) Development for Finite Element Modeling 14

Constitutive Model Defining the Point of Short-Circuit 14

1.3 Goals of the Current Research 14

Phase 1: 15

Phase 2: 15

Phase 3: 15

1.4 Prismatic Pouch Lithium-ion Cell Specifications and Mode of Failure 16

Cell Sizes, Chemistries, and Capacities 16

Cell Construction 16

Cell failure 17

1.5 Thesis Organization 18

2.0 Compression/Indentation of Low SOC Prismatic Pouch Cells 19

2.1 Introduction 19

2.2 Equipment Setup and Test Matrix 19

2.3 Test Results 21

Flat Compression Testing 21

Indentation Testing with Hemispherical and Conical Punches 23

2.4 Application to the Finite Element Model 29

2.5 Conclusions and Recommendations 29

Conclusions 29

Recommendations 30

3.0 SOC versus Thermal Runaway for Large Prismatic Pouch Cells 31

3.1 Introduction 31

3.2 Experimental Setup 32

Test Stand 32

Prismatic Battery Cells 33

Test Plan 34

3.3 Test Results 35

Hemispherical Punch Tests 36

Conical Punch Tests 37

Flat Compression Tests 39

3.4 Observations and Conclusions 39

4.0 Uniaxial Tension Tests of Cell Components for Material Characterization. **41**
4.1 Introduction 41
4.2 Equipment Description 42
Instron Test Machine *42*
Specimen Templates *42*
Digital Image Correlation System *43*
4.3 Test Material Description 44
Anode Layer *45*
Cathode Layer *45*
Separator Layer *46*
4.4 Test Setup 46
4.5 Test Execution and Results 46
Anode Layer *47*
Cathode Layer *47*
Separator Layer *48*
Four-Layer Tests *49*
4.6 Lessons Learned 52
Digital Image Correlation *52*
Specimen Cutting *53*
Eccentricity of Test Stand Grips *54*
Paint Speckling for DIC *55*
4.7 Conclusions and Recommendations 56

5.0 Thesis Conclusions and Recommendations for Future Work **57**
Conclusions 57
Future Work 57

References **59**

List of Figures

Figure 1: Internal construction of a large prismatic pouch cell. 17
Figure 2: Test machine and control station for prismatic pouch indentation tests, MIT ICL. 20
Figure 3: Flat compression testing of medium size prismatic pouch cells. 21
Figure 4: Results of flat compression tests on small and medium pouch cells..... 22
Figure 5: Flat cylindrical punch indentation test, large pouch cell..... 22
Figure 6: Flat cylindrical punch indentation of large pouch cell compared to analytical fit. 23
Figure 7: Punch sizes for local indentation, 90-degree conical, hemispherical punches..... 24
Figure 8: Test set up for small hemispherical punch with medium pouch cell. 24
Figure 9: Example of pouch inflation following indentation for small pouch cells. 25
Figure 10: Pouch inflation, indentation of medium cells with hemispherical punches. 25
Figure 11: Appx. zero %SOC large pouch cells, negligible inflation following indentation. 26
Figure 12: Load-displacement curves for small, medium, and large pouch cells. 26
Figure 13: Voltage vs. time for indented small, medium, and large pouch cells..... 27
Figure 14: Change in temperature vs. time for small, medium, and large pouch cells..... 27
Figure 15: Soft and hard internal short circuit for conical indentation of large pouch cell. 28
Figure 16: Peak load and deformation depth at short circuit vs. punch diameter..... 29
Figure 17: Test machine arrangement.....32
Figure 18: Inside test machine enclosure. 33
Figure 19: Large prismatic pouch cell ready for testing. 34
Figure 20: Typical results of 100% SOC punch test on large pouch cell. 36
Figure 21: Load, voltage, and surface temperature vs. time for hemi punch tests. 37
Figure 22: Load, voltage, and surface temperature vs. time for conical punch tests. 38
Figure 23: Test stand and control station for uniaxial tension tests. 42
Figure 24: Specimen template specifications, three templates with cutting tools. 43
Figure 25: Cell separator specimen at two levels of tension, overlaid with DIC. 44
Figure 26: Conceptual drawing of anode layer. 45
Figure 27: Conceptual drawing of cathode layer. 45
Figure 28: Typical cell separator material at high magnification. 46
Figure 29: Comparison of plain copper foil to copper anode in uniaxial tension..... 47
Figure 30: Comparison of plain aluminum foil to aluminum cathode in uniaxial tension. 48
Figure 31: Comparison of separator layers in MD and TD, uniaxial tension. 48
Figure 32: Drawing of four-layer test specimen with light paint speckling for DIC. 49
Figure 33: Four layer specimen installation into test grips using business cards. 50
Figure 34: Typical results of four-layer specimens in uniaxial tension. 50
Figure 35: Plots of component layers used to model four-layer specimen test results. 51
Figure 36: Comparison of four-layer specimen result to summed individual layer result. 52
Figure 37: High magnification view of specimen edge for straight and curved cuts. 54
Figure 38: Illustration of grip misalignment. 54

(This Page Intentionally Blank)

List of Tables

Table 1: Properties of small, medium, and large prismatic pouch cells. 16
Table 2: Summary of indentation tests performed by cell type. 20
Table 3: Test summary. 35
Table 4: Charged cell test result summary 40

List of Acronyms and Abbreviations

Ah	Ampere-hours
CT	Computerized (Axial) Tomography
DIC	Digital Image Correlation
EMI	(Fraunhofer) Ernst-Mach Institut, Germany
FEM	Finite Element Model
ICL	Impact and Crashworthiness Laboratory, MIT
kN	Kilonewton
Lp	Parallel Length (of test specimens)
mAh	milliAmpere-hours
MD	Machine Direction
MEMS	Microelectromechanical Systems
MIT	Massachusetts Institute of Technology
mm	Millimeter
MPa	Megapascal
RVE	Representative Volume Element
SOC	State of Charge
%SOC	Percent State of Charge
TD	Transverse Direction

(This Page Intentionally Blank)

Acknowledgements

The author thanks the following individuals for their assistance in completing this thesis:

First and foremost, Mrs. Kimberly K. Meier, for her undying love and support, and for taking care of just about everything not academic in nature during my three years of study and research at MIT. Without her selfless devotion to our family, this academic work would not have been possible.

Professor Tomasz Wierzbicki for his confidence in my abilities, technical guidance, and enthusiasm for this work. His wisdom and expertise are fundamental to the continued success of the Impact and Crashworthiness Lab at MIT.

Dr. Elham Sahraei Esfahani for her efforts in coauthoring two academic papers, research direction, and assistance in making sense of some of my results. Her expertise in Finite Element Modeling, data interpretation, and ability to recognize the way ahead for further research are invaluable to the research of Lithium-Ion batteries by the MIT Impact and Crashworthiness Laboratory.

CAPT Mark Welsh and CAPT Mark Thomas for their advice and leadership as supervisors of the 2N Naval Construction and Engineering Program during my time at MIT.

Dr. Manfred Salk, Dr. Thomas Kisters, and Mr. Frank Huberth of the Fraunhofer Ernst-Mach-Institut (EMI) Germany for their hospitality, and making their outstanding testing facilities and technical expertise available to me while completing the second phase of this project.

(This Page Intentionally Blank)

1.0 Introduction

1.1 Motivation for Research

Lithium-ion batteries are coveted for their small size, high energy density, rapid recharge rates, and low maintenance requirements. While the rates of catastrophic failure resulting in property damage and personal injury have been thus far statistically low, lithium-ion batteries are not without such risks. Lithium battery technology has been in military use for over a decade because of the energy density they provide, and the inherent risks that came with them are, to some extent understood by those that operate the lithium-ion powered equipment. As an example of efforts to mitigate the risks, the author points out that the U.S. Navy developed a technical manual for the technology [1], which outlines safety procedures and operator responsibilities for the use of lithium-ion batteries. To put the risk in perspective, it is worthwhile to note that the manual was prepared by the Naval Ordinance Center. While the technology does impose potential dangers due to the high energy packed in such a small volume, the author does not wish to convey that lithium-ion technology should be eliminated because of those dangers. Gasoline is also a dangerous technology, however prudent methods of storage and dispensing have made safe daily use as a source of power commonplace.

In recent years, lithium-ion battery technology has rapidly migrated into consumer product applications. As each year passes, the number of consumer and industrial grade products powered by lithium-ion batteries grows at a staggering rate. In October 2011, the number of portable electronic devices in the United States (most powered by lithium-ion technology) exceeded the number of people living there [2]. Several cases of cell failure have been reported in which cells used in portable electronic devices have suffered thermal runaway during use or recharging, resulting in high cell temperatures and even fires. These incidents have lead to manufacturer recalls of some cells [3, 4]. Because consumers cannot be expected to follow the same precautionary rigor when operating devices with lithium ion batteries as the Navy for example, industry has mitigated the risks somewhat by limiting the size of the cells and housing them inside robust packaging. But, today we are seeing the use of the technology expanding into larger-scale applications, to include power supplies for critical aircraft electronics and instrumentation, and as a primary power supply in electric automobiles.

While the likelihood that a battery cell located within a cellular phone would suffer impact or indentation damage is low, the same cannot be said for a large battery pack located inside a high-speed vehicle, such as an automobile or an aircraft. With the increasing use of lithium-ion technology in vehicular applications, the need to study the effects of abuse (impact) to the cells is amplified. While a great deal of research and reporting has been completed on the optimization of the technology from an energy density perspective, comparatively little research has been done on the effects of impacts or collisions in transportation applications.

Recently, there have been some significant incidents involving the failure of lithium-ion batteries in such vehicles. In April of 2012, an electric vehicle experimental battery pack exploded during controlled abuse testing at a General Motors facility resulting in personal injury and equipment damage [5], and in June of 2011 a Chevrolet Volt sedan caught fire following a NHTSA vehicular impact test that had occurred two weeks prior to the fire [6]. Events like these are the impetus for the MIT Impact and Crashworthiness Laboratory to conduct abuse testing on lithium-ion battery cells.

1.2 Related Research (2010-2012)

Research in this area by the MIT Impact and Crashworthiness Lab began in 2010 and is ongoing. The following sub-sections describe previous ICL research as outlined in prior-student theses:

Representative Volume Element (RVE) Development for Finite Element Modeling
In 2011, Richard L. Hill published the first thesis [7] and co-authored papers with Dr. Elham Sahraei and Dr. Tomasz Wierzbicki [8, 9, 10]. The motivation for the thesis was the argument that the lithium-ion battery manufacturing industry was using a design-build-test method to develop the technology, a method that has largely been abandoned by most other industries. The team argued that development and testing costs could be reduced and personnel safety improved by employing a robust computer finite element model (FEM) to accurately predict cell damage and short circuiting rather than conducting numerous physical tests. To minimize the processing power and computational time required to run the models, Hill and Sahraei conducted cell material characterization tests on small cylindrical and prismatic pouch cells, the results of which were used to create a representative volume element (RVE), which treated the cell model as a homogenized solid and, as a first-step showed good correlation with physical tests.

Constitutive Model Defining the Point of Short-Circuit
Continuing Hill's work, John E. Campbell published a thesis in 2012 [11] and co-authored papers with Sahraei and Wierzbicki [12, 13] reporting on mechanical tests performed for further validation of the FEM, along with additional tests to understand cell behavior following lateral compression and three-point bending for prismatic pouch cells, followed by indentation via rigid rods for small cylindrical cells. The research greatly improved the model and tests demonstrated that the point of short circuit following impact or indentation could be predicted.

1.3 Goals of the Current Research

In addition to continued refinement and validation of the FEM, the research conducted this academic year was exploratory in nature, with the goal of creating a list of topics that required further research in support of the overall lithium-ion battery effort at MIT, but also to develop testing methods and techniques to support it. The author's research can be categorically divided into three main branches or phases:

Phase 1:
This first phase involved uniaxial compression/indentation testing of medium and large prismatic pouch cells at low or zero percent state of charge (%SOC). There were three primary goals:

- Gain familiarity with the test equipment and test execution.
- Compare data obtained from medium and large cells to small cell data complied by Campbell and Hill to show trends.
- Report on the mechanical conditions (load) required to cause cell internal short circuit.
- Use the baseline load displacement data for the large cells for comparison to Phase 2 work.

Phase 2:
In the second research phase, the author conducted indentation tests on large prismatic pouch cells at various %SOC. The goals of this research were as follows:

- Determine the extent of cell damage resulting from punch impact as a function of %SOC.
- Assess any correlations in load/displacement, peak temperature, and rate of thermal runaway as a function of punch type or %SOC.
- Determine if any correlations not previously identified exist.
- Determine a future test plan for charged cells.
- Compare the results to those obtained from zero %SOC testing completed at MIT (Phase 1).

Phase 3:
The third and final phase of the research shifted from a global reference point to a local one. Samples of dry components (anode, cathode, and separator) were tested in a uniaxial tension test machine for material characterizations in an effort to create a more robust FEM that accounted for the different layers within the cell. This would permit adjustment to the model to account for different chemistries. The specific goals of my research were:

- Gain familiarity with the new test equipment and test execution.
- Develop methods to create suitable test specimens of the extremely delicate cell layer materials.
- Develop techniques to test the specimens without damaging them during installation into the test machine.
- Utilize digital image correlation (DIC) equipment to measure specimen strain during the tests.
- Determine the effect of the anode and cathode coating on specimen stress and strain by comparison to uncoated foil samples.

1.4 Prismatic Pouch Lithium-ion Cell Specifications and Mode of Failure

The terms "small", "medium", and "large" are used liberally throughout this thesis to describe the different prismatic pouch cells tested. This section provides details regarding the dimensions and chemistries and basic construction of each type, as well as a description of how these batteries fail when abused.

Cell Sizes, Chemistries, and Capacities

Cell properties are presented in Table 1. The cells ranged from 59mm (small) to 227mm (large) in length, with nominal capacities of 740 mAh up to 19.5 Ah. Three different chemistries are involved: $LiCoO_2$, $LiMnNiCoO_2$, and $LiFePO_4$.

	Small Pouch Cell	Medium Pouch Cell	Large Pouch Cell
Nominal Capacity	740 mAh	3.2 Ah	19.5 Ah
Nominal Voltage	3.7 V	3.7 V	3.3 V
Thickness	5.35 mm	8.2 mm	7.25 mm
Width	34 mm	43.5 mm	160 mm
Length	59.5 mm	129.5 mm	227 mm
Weight	19 g	85 g	496 g
Chemistry	$LiCoO_2$	$LiMnNiCoO_2$	$LiFePO_4$

Table 1: Properties of small, medium, and large prismatic pouch cells.

Cell Construction

Figure 1 shows a typical large prismatic pouch cell assembly before it is vacuum packaged in a sealed pouch with electrolyte. Layers of anode and cathode sheet are alternately stacked between accordion-folded layers of separator, which electrically insulates anodes and cathodes from one another. The anodes and cathodes are electrically fastened together by means of spot welds at the terminal ends. A final layer of separator envelops the completed stack.

Following assembly, solid terminal ends are installed and the stack is inserted into a Mylar pouch, which is placed in a vacuum sealing machine and heat-sealed shut. The pouch is capable of venting built-up gas in the event of catastrophic failure by rupture of one of the seams on the pouch.

To increase durability, the pouch cells are commonly housed in a tough protective casing, either individually or in multiples to make a battery pack.

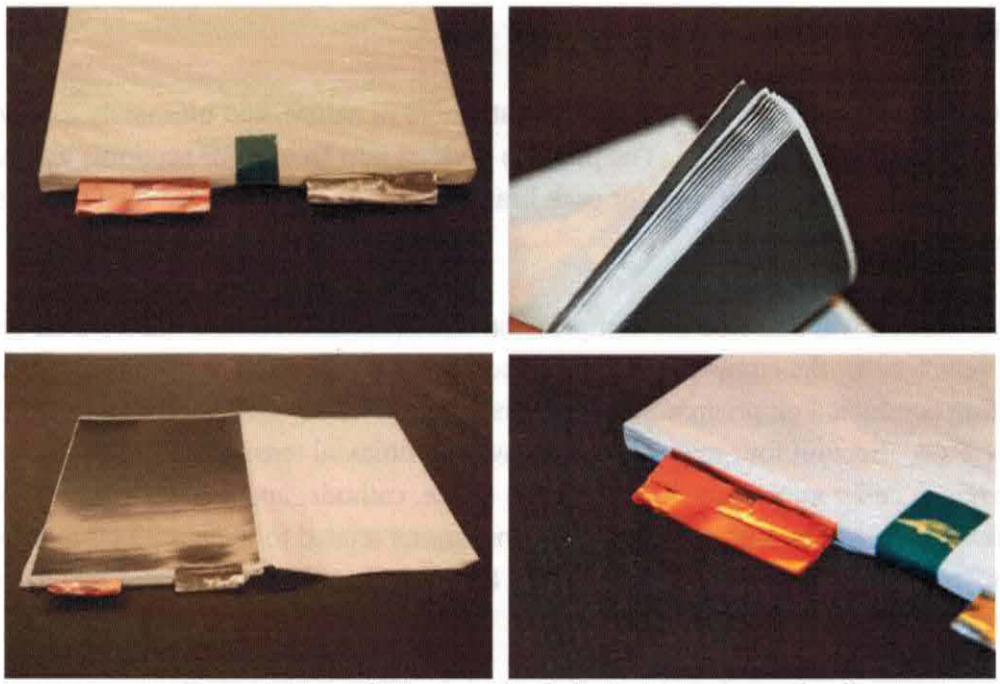

Figure 1: Internal construction of a large prismatic pouch cell.

Cell failure

In order to describe the damage that a loaded cell undergoes, a definition for "cell failure" was required. For the battery compression and indentation tests conducted for this thesis, "cell failure" is defined as the point at which a departure from steady terminal voltage is noted (i.e. short-circuit). The short can occur for multiple reasons, to include shorting the cell across its terminals, impurities internal to the cell creating a path for current flow between layers, or indentation of the cell from an external source. Great care is taken to prevent shorting battery terminals either in the handling of individual cells or in the design of battery casings to preclude such incidents. The separator layer in these cells is as thin as 25 microns (25 μm), so very strict cleanliness controls are required during assembly. A tiny granule or sliver of metal could perforate the separator and lead to an internal short circuit. While challenging, this level of cleanliness is not impossible and failures of this type are statistically few. This research looks at the last method, which is the most difficult to anticipate since a vehicle could be impacted in a large number of ways.

Cell failures from indentation testing are repeatable and simple to detect. Generally, at the point of voltage drop, a prompt drop in punch load and gradual rise in cell surface temperature also occur. It is postulated that the prompt drop in punch load is due to a local failure of one or more of the individual layers within the cell, which allows two or more of the anode/cathode layers to come into direct contact resulting in the short circuit. The rise in surface temperature comes from the release of energy chemically stored in the cell. The process of release is called thermal runaway. The temperature rise is partially a function of SOC, and fully charged cells can undergo such rapid thermal runaway that pouch rupture and vaporous electrolyte venting occurs.

1.5 Thesis Organization

The research conducted for this thesis was investigative in nature, and ultimately explored three separate but related areas of study. The paper is divided into five major sections: an introductory section, three research sections (one for each branch of the study) followed by a conclusion and recommendation section.

The second section will describe the compression and indentation tests conducted on discharged prismatic pouch cells, the equipment used, and test results. The third section provides details on abuse testing conducted on prismatic pouch cells with different %SOC and associated thermal runaway effects. Section four reports on the results of uniaxial tension testing performed on prismatic pouch cell components, to include the anode, cathode, and separator layers. While sections two through four will have separate conclusions related to the particular research described, section five draws conclusions about the overall study and provides recommendations for further research.

2.0 Compression/Indentation of Low SOC Prismatic Pouch Cells

Shortly after completion of this phase of the research, a report of these tests and their application to Dr. Elham Sahraei's computational battery models were submitted to the Journal of Power sources for publication. This paper is cited as Reference [14].

2.1 Introduction

As the application of lithium-ion batteries further expands into the vehicular market, the need to understand the effects of their exposure to varying speeds and accelerations becomes more critical. The difference between these applications and those used in consumer electronics is that the moving battery is exposed to local forces and deformations that in extreme cases, such as in a vehicle crash, can result in local damage to the cell. Excessive damage can ultimately cause an internal short circuit, even if the exterior casing of the cell does not fail or fracture. Such short circuits inside a battery pack can result in the venting of toxic and flammable vaporous electrolyte or even a fire, as outlined in [6, 15] and discussed in detail in Section 3.0 below.

The need to better understand the behavior of batteries under mechanical loading and the conditions that lead to an electric short circuit has motivated the current research, which continues the work of Hill, Campbell, Sahraei, and Wierzbicki, as summarized in Section 1.3 of this thesis and in journal articles [12, 13, 14]. The only publications known to the author on mechanical properties leading to short circuit in a cell are from Sahraei et al, Wierzbicki and Sahraei [14], and Greve and Fehrenbach [16].

The current study complements the earlier works by providing test results on two additional types of prismatic pouch lithium ion cells. The tests were designed to report on the mechanical conditions leading to development of an electric short circuit in those cells, and combined with data complied by Campbell in 2012 [11], demonstrate that the current homogenous and isotropic constitutive model of the jellyroll is suitable for a range of battery chemistries, cell sizes, and loading conditions.

2.2 Equipment Setup and Test Matrix

Three types of prismatic pouch cells were used for this research: small, medium, and large. Properties of these cells are presented in Table 1 of Section 1.4 above. The research team requested that cell manufacturers discharge the cells to 10% or less SOC to prevent extreme reactions during the indentation tests. Table 2 provides a summary of the tests performed on these cells. Note: Campbell completed testing on small cells in 2012 [11], but test descriptions and results from those tests are, in part, included here for comparison.

Cell Type	Tests Performed
Small Cell	Flat compression between two plates. (Sahraei et al 2012)
	Indentation with small, medium, and large hemispherical punches and 90-degree conical punch. (Sahraei et al 2012)
Medium Cell	Flat compression between two plates.
	Indentation with small, medium, and large hemispherical punches and 90-degree conical punch.
Large Cell	Indentation with small, medium, and large hemispherical punches, a flat cylindrical punch, and a 90-degree conical punch.

Table 2: Summary of indentation tests performed by cell type.

In all cases, the pouch cells were tested using a 200 kN MTS compression/tension test machine. Load cells with a maximum range of 10 kN and 200 kN were available for the tests, and appropriately selected based on maximum anticipated test load in each case. Campbell gave a detailed description of the equipment in his 2012 thesis [11], so that information is not repeated here. The test machine arrangement with exhaust hood (left) and control station (right) is illustrated in Figure 2.

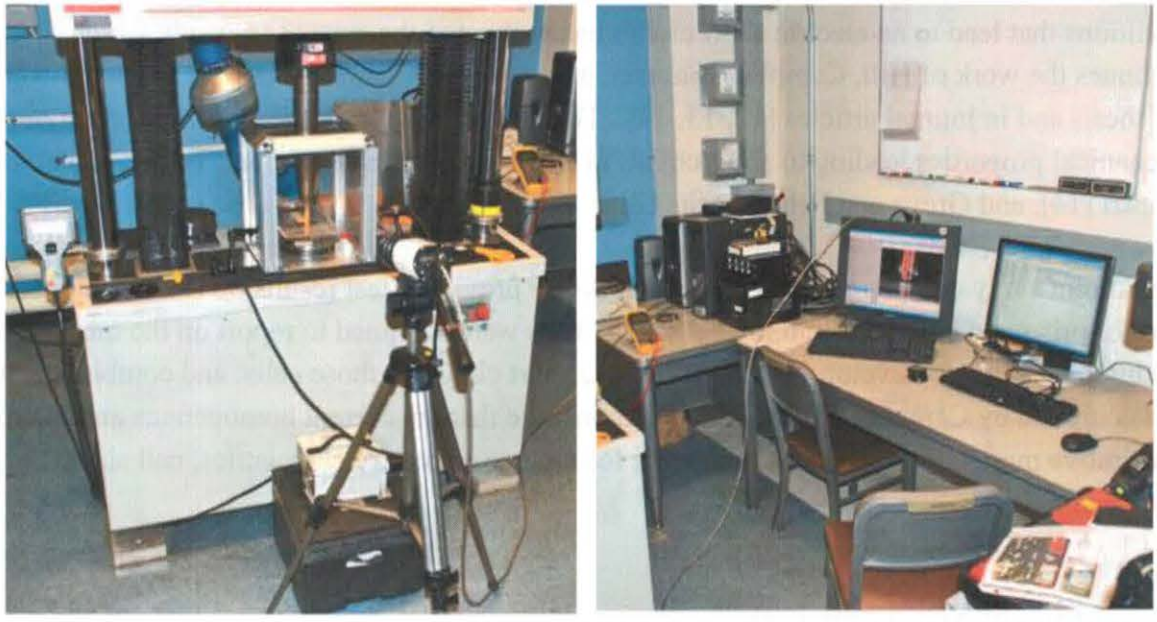

Figure 2: Test machine (left) and control station (right) for prismatic pouch indentation tests, MIT ICL.

Tests were conducted using a fixed displacement rate of one millimeter per minute (quasi-static), and continued until either the maximum load cell rating was reached, or the cell showed evidence of an internal short circuit, as described in Section 1.4. The following parameters were measured and recorded at one-second intervals to a desktop computer:

- Test machine load and crosshead displacement.
- Cell voltage over time, measured with a typical voltmeter at the cell terminals.
- Cell surface temperature over time, monitored via thermocouple.
- Photographs of the cell at the punch site, at a rate of one image per second.

Once short-circuit was achieved, temperature and voltage monitoring continued until those parameters returned to a steady-state condition.

2.3 Test Results

Flat Compression Testing

Flat compression tests on small pouch cells were previously reported by Sahraei et al [13] and the results of those tests were used to calibrate a finite element model of the small cell. In this series of tests, a medium pouch cell was placed flat between two 8-inch platens in a test machine with voltage and temperature measurement devices attached as described in Section 2.2. Figure 3 shows the arrangement.

Figure 3: Flat compression testing of medium size prismatic pouch cells.

The cell exhibited stable voltage and temperature through the test. Compression was halted when the maximum safe load limit of 190 kN for the test machine was reached. Following compression, an inspection of the cell showed that much of the electrolyte that was initially between the layers had been squeezed out to the periphery of the layer stack as evidenced my long blisters in the Mylar along the stack edges. The pouch did not rupture or leak electrolyte. Figure 4 gives the load-displacement results of the test with the earlier small-cell results included for comparison.

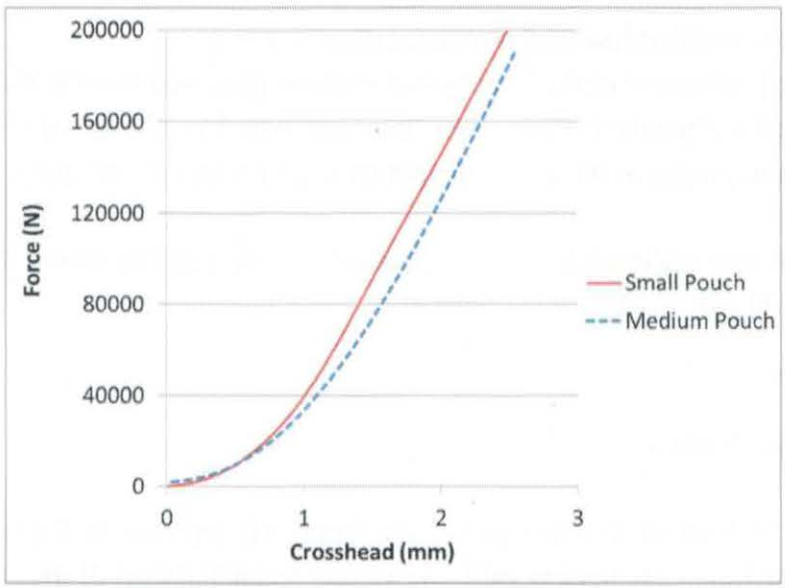

Figure 4: Results of flat compression tests on small and medium pouch cells.

A flat compression test on a large cell could not be performed with the available equipment due to platen size and force limitations. Instead, a test was performed on a large cell using a 25.31 mm diameter flat cylindrical punch. Figure 5 illustrates the test, and force - displacement results are reported in Figure 6.

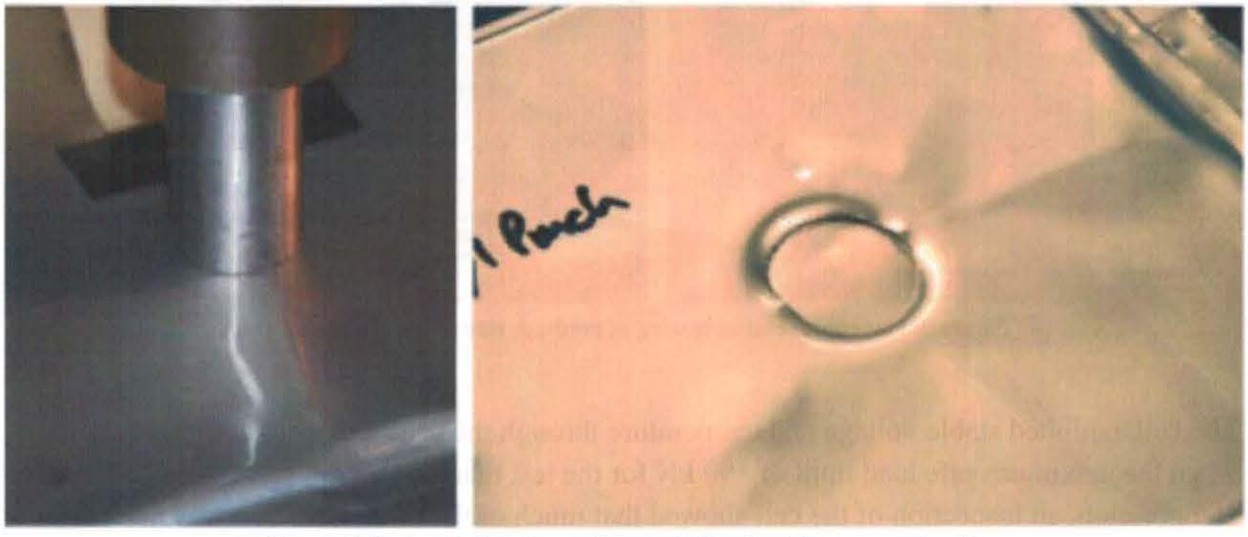

Figure 5: Flat cylindrical punch indentation test, large pouch cell.

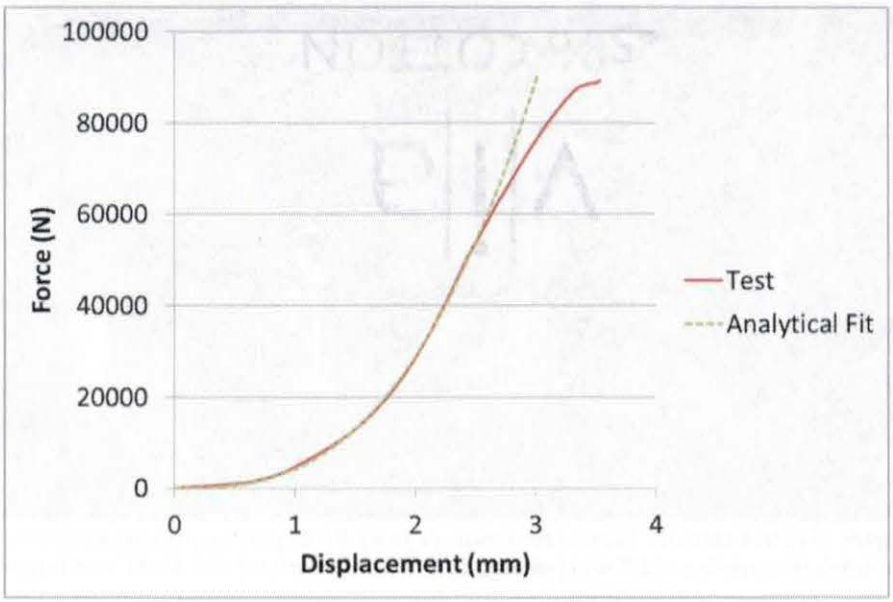

Figure 6: Flat cylindrical punch indentation of large pouch cell compared to analytical fit.

In the case of the flat cylindrical punch test, it can be seen that the sharp edges of the punch surface actually cut the cell pouch and likely one or more layers inside; therefore, the ensuing short circuit is more likely a result of the cut than from the stress-strain state within the cell. From the result graph, we see that the cutting of the pouch results in disparity between reality and theory. Since this test did not yield information useful to FEM calibration, no further tests using this punch were conducted. In more recent tests performed in collaboration with Fraunhofer EMI and reported in [17] and Section 3.3 of this thesis, large cells were compressed between two flat plates up to 500 kN and exhibited no reduction in capacity when discharged and recharged after the test. It can be concluded that uniform flat compression of pouch cells will not lead to electric short circuit; however, such a uniform load is not likely to occur in real life accident events. Therefore, the remaining tests served to simulate more local loads. Still, the flat compression tests provided needed information to calibrate the constitutive equations.

Indentation Testing with Hemispherical and Conical Punches

Subsequent to the calibration tests, a comprehensive test program was conducted to validate the corresponding models. The three types of cells were indented with a series of punches: three hemispherical (small, medium, and large) and one conical shape. Figure 7 shows the punches used and give dimensional data.

Figure 7: Punch sizes for local indentation, (L to R), 90-degree conical, hemispherical punches of diameters 12.7 mm (small), 28.575 mm (medium) and 44.45 mm (large).

The punches were positioned over the center of the cell lengthwise and widthwise, and a thermocouple was attached to the top surface of the cell with adhesive, approximately one inch from the punch footprint, to prevent damage to the sensor. The top surface was chosen over the bottom side to eliminate masking of true surface temperatures caused by heat conduction between the cell and the steel base plate of the test machine. Voltage was continuously measured directly from the cell terminals. Figure 8 illustrates the test setup using a medium sized cell and small hemispherical punch.

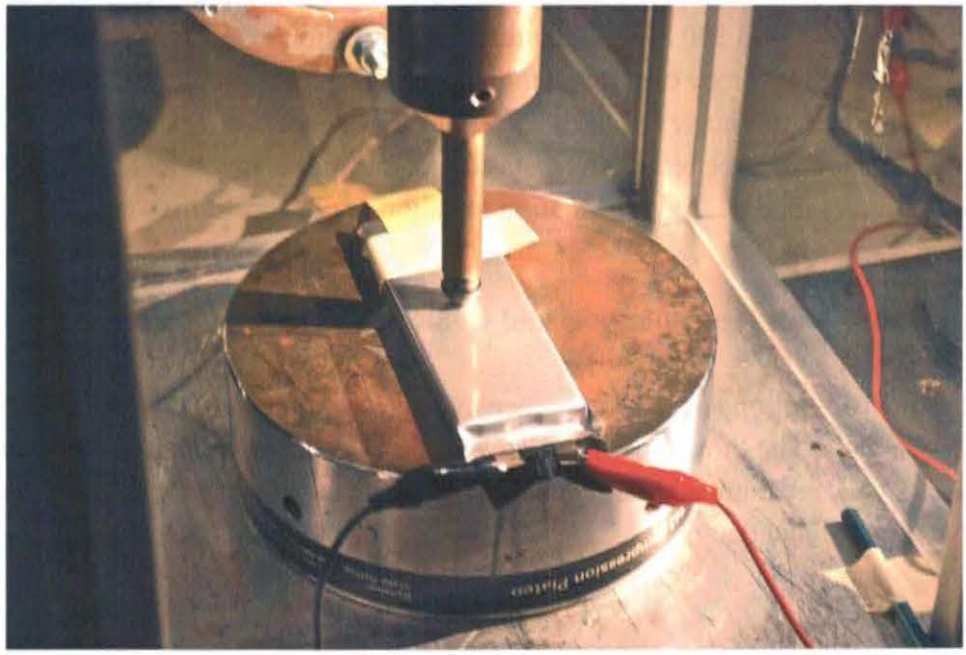

Figure 8: Test set up for small hemispherical punch with medium pouch cell.

Upon short circuit in any of the indentation tests, observed were a simultaneous drop in force, drop in voltage, and increase in surface temperature. The small and medium cells exhibited pouch inflation due either to formation of gases from short-circuit chemical reactions or vaporization of the cell electrolyte. Comparisons of small cells before (left) and after (right) indentation are shown in Figure 9.

Figure 9: Example of pouch inflation following indentation for small pouch cells.

Figure 10 offers a similar comparison for the medium sized cells. The inflation was more intense for the case of medium cells, suggesting the cells had a %SOC greater than ten. In the top-right image of Figure 10, electrolyte leakage can be seen as a reddish liquid collecting along the long-edge seam of the battery cell.

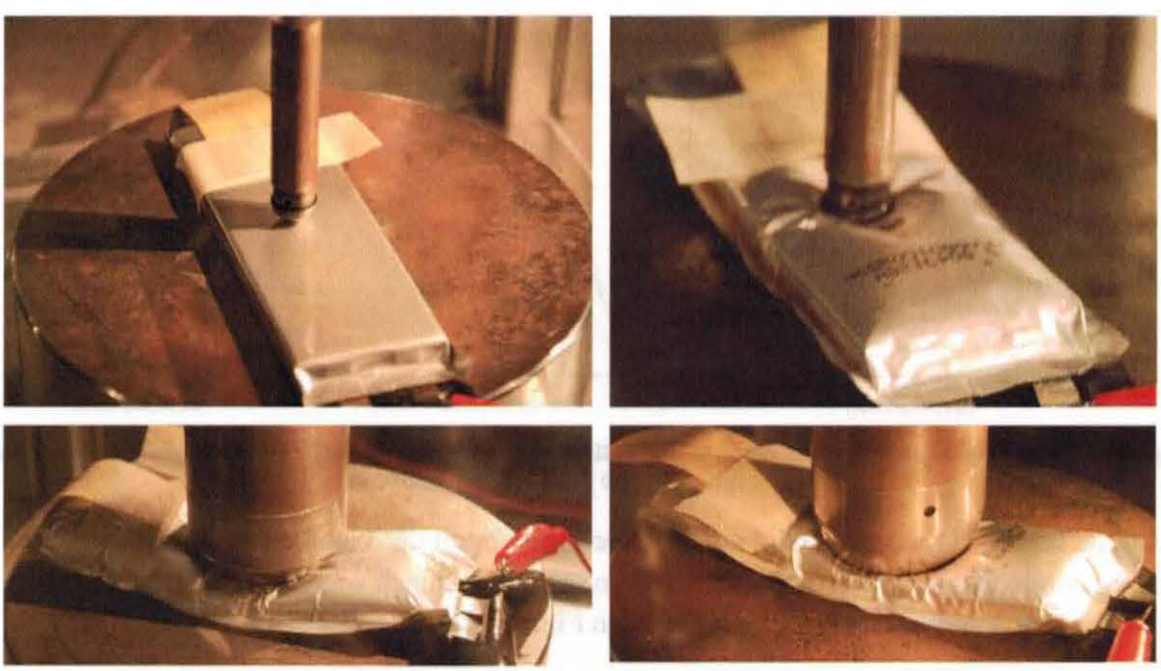

Figure 10: Example of pouch inflation following indentation of medium pouch cells with small (top) and large (bottom) hemispherical punches.

The large cells proved to have a %SOC close to zero, and exhibited almost negligible temperature increases as a result of the indentations. Only slight expansion localized to the indentation point resulted, otherwise the large cells showed no inflation, see Figure 11.

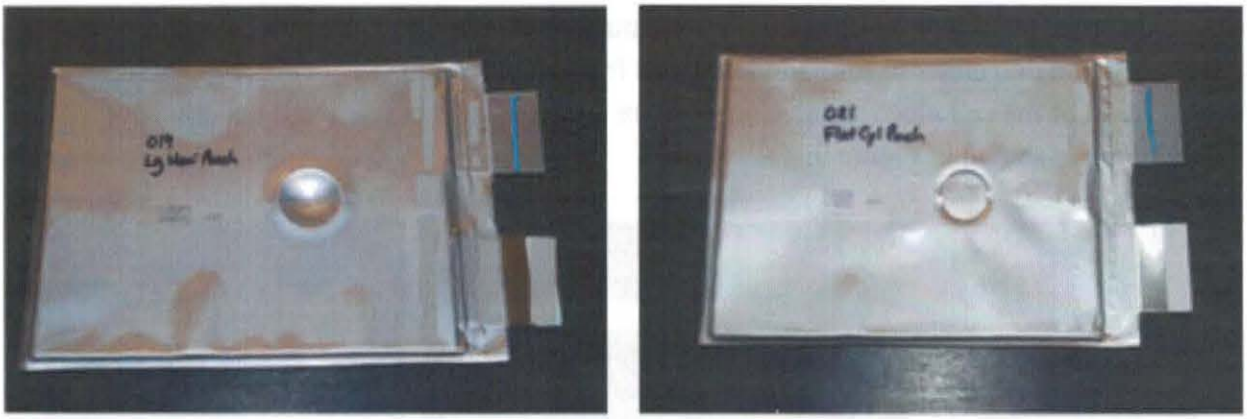

Figure 11: Approximately zero %SOC large pouch cells showing negligible inflation following indentation.

For all three types of cells, there was a consistent, progressing pattern for the load-displacement curves with different punch sizes, meaning that the peak load at short circuit increased with an increase in punch diameter, as shown in Figure 12.

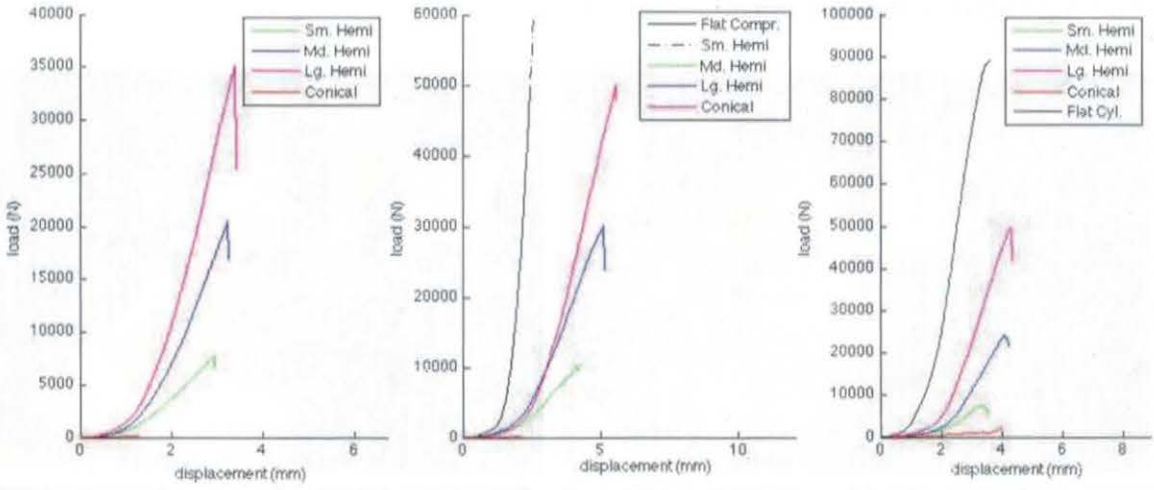

Figure 12: Load-displacement curves for (L to R) small, medium, and large pouch cells. The onset of short circuit corresponds to the peak load for each test.

The large hemispherical punch did not produce short circuit until load exceeded 30,000 N for any cell, while the peak force at short circuit for a conical punch was less than 0.1% of that value, making it difficult to see (the red line) in Figure 12.

The rise in temperature and drop in voltage at short circuit versus time for all punch sizes are shown in Figures 13 and 14. It can be observed that the short circuit is delayed with an increase in diameter of the punch. The peak temperature at short circuit decreases from medium to large punch size for all three cells, but the peak temperature for conical and small punch sizes did not follow a similar consistent trend.

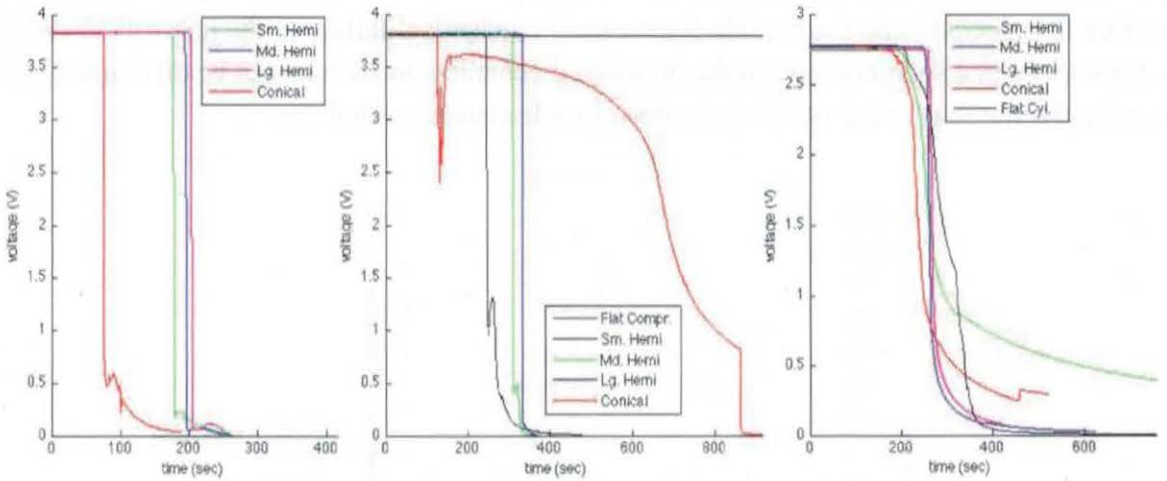

Figure 13: Voltage vs. time for indented (L to R) small, medium, and large pouch cells.

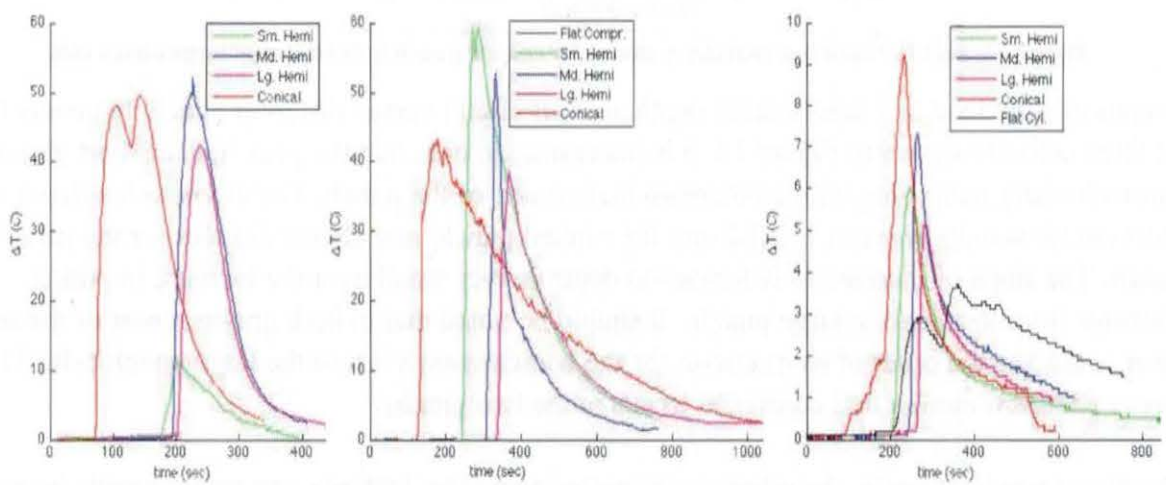

Figure 14: Change in surface temperature vs. time for indented (L to R) small, medium, and large pouch cells.

The short circuit of the large cell with a conical punch had a distinct feature, see Figure 15. Two separate phases could be observed. In the first phase, at a displacement of about 1.3 mm, a small local peak was observed in the force (highlighted with a circle in the figure), while at the same time a small rise in temperature to about 0.5 °, and a slight drop in voltage of about 0.5 V was observed. This drop in voltage was not noticeable in the full-scale plots. The loading continued, which resulted in three more small peaks in load and subsequent small steps of increase in temperature and decrease in voltage. In the second phase, at a force of 1200 N, a more distinct drop in force can be observed, and was accompanied by a significant drop in voltage and rise in

temperature. These two phases could be distinguished as "soft" and "hard" internal short circuits. What is remarkable is that even the soft short circuit is initiated with a local peak in the force and therefore is expected to be predictable from a local mechanical failure in the jellyroll. A cell that has gone through a soft short circuit due to small mechanical loads may not be distinguishable immediately, but may cause delayed reactions in subsequent normal use.

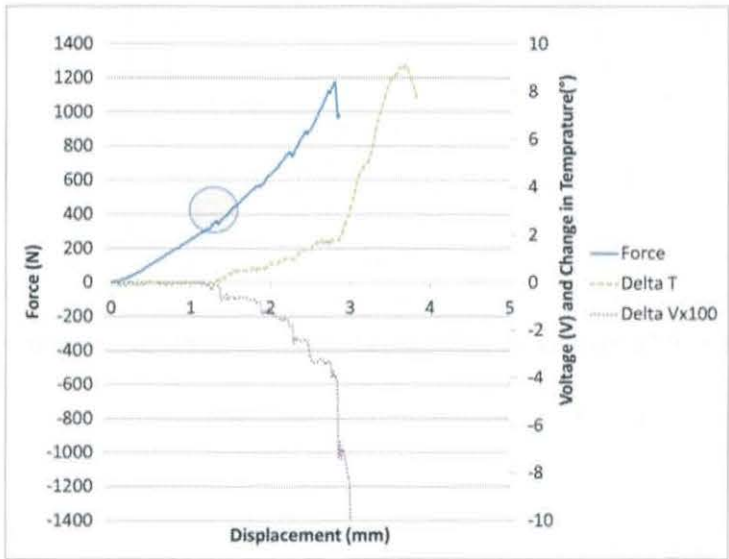

Figure 15: Soft and hard internal short circuit for conical punch indentation of large pouch cell.

Graphs of peak load and deformation depth at short circuit versus different punch diameters for all three cells are shown in Figure 16. It is interesting to note that the peak load at short circuit is almost linearly increasing with an increase in diameter of the punch. The deformation depth at short circuit is only between 1 and 2 mm for conical punch, and almost doubles for the small punch. The slope of increase in deformation depth is very small over the increase in punch diameter from the small to large punch. It should be noted that in both graphs, onset of the **soft** short is used as the onset of short circuit for the conical punch test of the large pouch cell. The three cells show similar and consistent trends in the two graphs.

The above results quantify the otherwise expected trend that batteries can safely handle increases in intrusion as the objects become more blunt. No failure was observed for compression between two flat plates, which corresponds to an infinite punch radius.

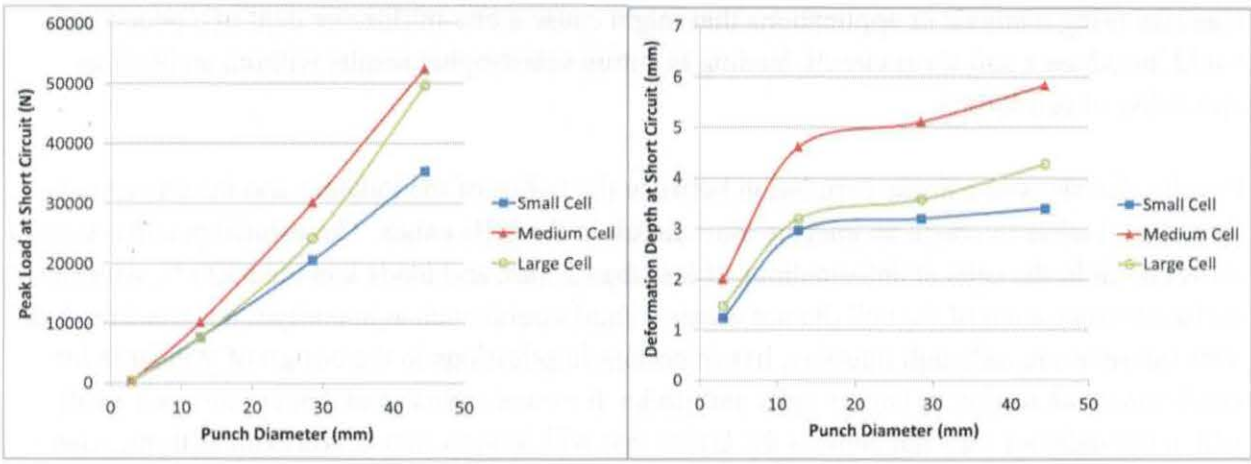

Figure 16: Peak load (left) and deformation depth (right) at short circuit vs. punch diameter.

2.4 Application to the Finite Element Model

Following the physical testing, Dr. Elham Sahraei used analytical procedures to extract material and mechanical properties of the cell. Then, a finite element model of each cell was developed and the calibrated material properties were entered. The model accurately predicted the load, displacement, and deformation profile of the cell as well as conditions leading to electric short circuit in each cell. A detailed analysis of this effort is offered in reference [14], and will not be repeated here.

2.5 Conclusions and Recommendations

Conclusions

An experimental compression and punch indentation program was completed on three types of pouch cells to understand their mechanical behavior under mechanical loading, and to investigate conditions leading to internal short circuit. It was observed that under all punch indentation tests, short-circuit was consistently detected by a simultaneous local peak in force, drop in voltage, and rise in temperature.

In a test of conical punch indentation of large pouch cells, a soft short circuit preceded a complete, or hard short circuit; still the soft short was detectable with the same features of drop in force, voltage, and rise in temperature. Although the magnitude of the changes in force, voltage, and temperature in case of soft short were significantly smaller than the complete short circuits observed in other cases, the peak force and deformation at soft short was within expected values based on the trends observed in all other cases. This is a significant finding, as it means from the extent of deformation alone, one can predict possible existence of a soft short inside a cell, even if the voltage of the cell does not indicate an internal short circuit. It means that

manufacturing methods or applications that might cause a one-millimeter dent in a pouch cell could introduce a soft short circuit, leading to future catastrophic results without an obvious indication of cell failure.

Results also showed a linear correlation between the radius of the indenter and the amount of force that it takes to create an interior short circuit in the cells exists. The conical punch created a short circuit in the cells at deformations of less than 2 mm, and loads less than 400 N, while a flat surface compression of the cell did not create a short circuit even at maximum test machine load. This information, although intuitive, has important implications in the design of standards for crash and crush testing of battery cells and packs. It means a crush test that compresses a cell with a flat indenter may not address the issues that will be seen in real-world conditions, where intrusion occurs asymmetrically and with narrower objects.

Recommendations

The method of vacuum packaging, the presence of toxic electrolyte, and the extremely delicate nature of the individual layers makes physical dissection of a tested cell to determine actual cause of short circuit extremely difficult. While prediction and recognition of short-circuit has been mastered at this point, the actual cause of short-circuit remains a mystery. Is the force of the punch causing the separator material to crack, allowing the anode and cathode to come in contact, or are tiny particles of the coating being forced through the porous separator until enough have passed to complete an electron path?

Based on the scale of the damage to the cells, the author recommends further investigation into this phenomenon at a microscopic level. Use of CT scans or electron microscopy might provide answers to such questions.

3.0 SOC versus Thermal Runaway for Large Prismatic Pouch Cells

Shortly after completion of this phase of the research, a report of these tests was submitted to the Proceedings of the Battery Congress 2013 for publication. This paper is cited as Reference [17]. The author wishes to thank the Fraunhofer Ernst-Mach Institut (EMI) for providing facilities and technical expertise used in the execution of this research.

3.1 Introduction

The rapid increase in utilization of lithium-ion batteries as a preferred power source has placed a large emphasis on cell abuse studies; however, most of those found in the literature do not address the limits of integrity in the case of mechanical abuse. While cell manufacturers assuredly perform such studies, the results are not published. In many applications, such as cameras and cell phones, the likelihood of impact damage is small; however in others, such as electric cars, a significant risk of impact damage to the battery pack exists. In order to improve cell package design and mitigate the potential hazards that these energy-dense cells pose in an impact, the behavior of charged cells following deformation must be understood.

As described in Section 1.4 of this thesis, a common mechanism of catastrophic failure for lithium–ion battery cells is thermal runaway caused by a short circuit between the anode and cathode layers of the cell, which can occur if the separator membrane is damaged and the anode and cathode layers are allowed to make contact. In order to study the effects of percent state of charge (%SOC) on thermal runaway, the cells must have a non-zero charge, and special testing equipment and facilities capable of containing high-energy cells undergoing catastrophic failure are required. A collaborative effort between MIT's Impact and Crashworthiness Lab and scientists and engineers from the Fraunhofer Institute for High-Speed Dynamics in Germany performed preliminary abuse testing on lithium-ion prismatic pouch cells at various %SOC. The objective of this study was fivefold:

- Determine the extent of cell damage resulting from punch impact as a function of %SOC.
- Assess any correlations in load/displacement, peak temperature, and rate of thermal runaway as a function of punch type or %SOC.
- Assess the effectiveness of selected parameter measurement methods used for the tests.
- Determine if any correlations not previously considered exist.
- Compare the results to those obtained from zero %SOC testing completed at MIT.

Since the study was of significant interest to the automotive industry, the prismatic pouch cell selected was of a size and capacity typically used in the construction of electric/hybrid vehicle battery packs. Preliminary testing was performed on zero %SOC cells at MIT for comparison to the charged cell results. Details of that work were described in Section 2.0 of this thesis.

3.2 Experimental Setup

Charged cell testing was conducted at a Fraunhofer EMI ballistic test facility in Kandern, Germany, where appropriate facilities were available to contain reactive cells, handle hazardous materials, and eliminate chances for personnel injury during experiments. Testing was confined to a two-week availability period.

Test Stand

The test stand consisted of a hydraulically operated, piston driven ram fitted with a load cell for force measurement and a precision displacement measurement device. Attached to the bottom of the ram was either a hemispherical or conically shaped indenter punch, or a set of compression platens, depending on the test. The ram passed through the top of a thick metal enclosure inside which the test specimen was positioned. Video footage of each test was recorded with standard high-definition and high-speed (1000 fps) cameras. Figure 17 shows the test stand external arrangement.

Figure 17: Test machine arrangement, courtesy Fraunhofer EMI.

The enclosure was fitted with a hinged front panel with a ballistic-glass viewing window to permit direct observation of the reaction. The enclosure also had test connections for monitoring cell surface and ambient air temperatures, atmospheric sampling, ventilation and exhaust hoses,

and video recording capability. Angled mirrors in the rear corners of the enclosure permitted the video cameras to record any visual cell response obscured by either the cell itself or the punch mechanism. An absorbent litter was placed in the bottom of the enclosure to soak up any liquid electrolyte that might leak from the cell during testing. Figure 18 shows the internal enclosure arrangement. The test machine and enclosure were housed in a bunker-type building with an adjacent control center that housed the computers and instrumentation needed to run the tests.

Figure 18: Inside test machine enclosure, courtesy Fraunhofer EMI.

Test specimens were placed within the enclosure such that the punch was centered over the cell. The test stand hydraulic cylinder provided a maximum load of 500 kN. Unlike the MTS tensile/compression test machine used in the earlier tests for discharged cells, which operate at a constant rate of displacement, this test stand operated via constant hydraulic pump discharge pressure, so punch speed was solely a function hydraulic pressure and the specimen's resistance to compression.

Prismatic Battery Cells

The cells used were the "Large" type described in Section 1.4. Figure 19 provides an illustration, showing voltage measurement leads and surface thermocouple attachment points. The cells were centered beneath the punch in the test enclosure such that the punch contacted the cell in between the attached surface thermocouples.

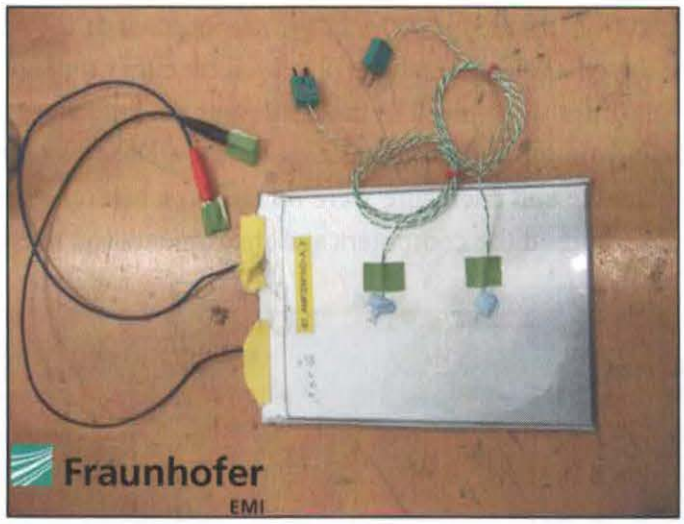

Figure 19: Large prismatic pouch cell ready for testing, courtesy Fraunhofer EMI.

Test Plan

Prior prismatic pouch cell impact testing was limited to the indentation of nearly discharged prismatic pouch cells. For many reasons, a formal testing plan was not developed for these exploratory experiments. Reasons included, but were not limited to the following:

- Limited lab availability (two weeks).
- Cost and availability of prismatic cells.
- Time required bringing cells to required %SOC.
- Time required to clean the test enclosure following cell reaction and cool-down period.
- Hazardous material concerns.

Of the five factors given, the time required to obtain proper state of charge, allowing for post-test cool-down, and clean up processes were the most time consuming. Depending on the test performed, as few as one test or as many as three tests could be completed in a given workday.

Ultimately, tests were conducted to measure the extent of reaction as a function of %SOC to determine if there was a threshold value of SOC where thermal runaway did or did not occur. Two different punch types were used. The first was a steel hemispherical punch of diameter 28.5mm. The second was a steel 90-degree conical punch. Both punches were manufactured to the same dimensional specifications as two of the punches used for the preliminary zero percent SOC tests conducted at MIT. In addition to the punch tests, flat-compression tests were conducted on one zero-percent charged, and one fully charged cell beneath a flat platen fitted to the test stand ram, to determine if a flat compression of 500 kN would result in any change in cell capacity.

Testing began with a 100% SOC cell, followed by a 50% SOC cell. The level of reaction observed for the 50% cell then determined whether the next test would be on a 75% SOC cell (no reaction at 50%) or a 25% SOC cell (high reaction at 50%). Table 3 summarizes the twelve tests completed.

% SOC	Hemi Punch	Conical Punch	Flat Compression
0	X	X	X
25	X	X	
50	X	X	
75		X	
100	XX	X	X

Table 3: Test summary, EMI tests.

Two specimens were tested at 100% SOC with the hemispherical punch to determine if results were in any way repeatable. A 75% SOC cell was not tested with the hemispherical punch due to high reaction at 50% SOC, time constraints, and cell availability.

3.3 Test Results

Following each test run, the high-speed video footage was reviewed for any visual clues as to how the onset of thermal runaway occurs, but no remarkable evidence was observed. The test enclosure provided for atmospheric constituent monitoring, but readings could only be obtained if the enclosure ventilation system was secured. Visual observation of the cell would then be obscured due to the large vapor emissions from the charged cells. For this reason, only the first test was performed without ventilation so atmospheric monitoring could be performed. The major constituent of concern in the vapor was found to be hydrogen fluoride. Because different atmospheric results were not anticipated and visual observation was more important, all subsequent tests were performed with the ventilation system operating.

Punch load, surface temperature, and cell voltage data were processed following the testing phase, and each was plotted against time. Because two surface temperature thermocouples were used, their outputs were averaged together for plotting. A direct comparison of the charged cell data to earlier tests conducted on discharged cells at MIT was not possible, as the test machine used for these tests was not a "continuous displacement rate" type. The differing mode of force caused displacement rate to vary, and smooth load/displacement plots could not be produced.

Figure 20 shows the typical physical result of a 100% SOC test for either the hemispherical or conical punch. By external inspection alone, there was no way to discern the results of one punch type over the other. When compared to Figure 19 above, it is obvious that the structure of the cell had been dramatically altered.

Figure 20: Typical results of 100% SOC punch test on large pouch cell, courtesy Fraunhofer EMI.

The right image in Figure 20 shows the side view of the cell with a ruptured seam and rippled anode and cathode layers. The clumps of light-colored material shown between the layers are singed or melted separator material. During higher energy tests (in excess of 50% SOC) the loud "pop" resulting from pouch rupture was clearly audible in the control room, indicating significant pressure built up within the pouch, despite perforation by the punch.

The left image in Figure 20 is a top view of the cell where the punch penetration into the cell can clearly be seen as well as some radial pouch tearing from the center of the penetration point. The ruptured seam shown on the right is at the bottom of the photograph on the left. Brownish staining from condensed electrolyte vapor residue is also visible on the pouch exterior.

Hemispherical Punch Tests

Figure 21 provides plots of load, voltage, and surface temperature versus time for tests using the hemispherical punch at various states of charge. As mentioned in Section 3.2, a second 100% SOC test was performed to see if results were repeatable, but the results from the second test did not show good correlation with the first. The research team anticipated that the results would show a trend of some kind, perhaps a higher load capacity as state of charge decreased, etc. however no such trend for any of the parameters was discovered with one exception. If the second 100% SOC test is ignored, it can be seen in the temperature plot that the peak surface temperatures and initial rates of temperature rise do trend as %SOC increases. This may be of limited significance, however, as the team later determined that surface temperature is likely not a good measurement method for determination of rate of thermal runaway.

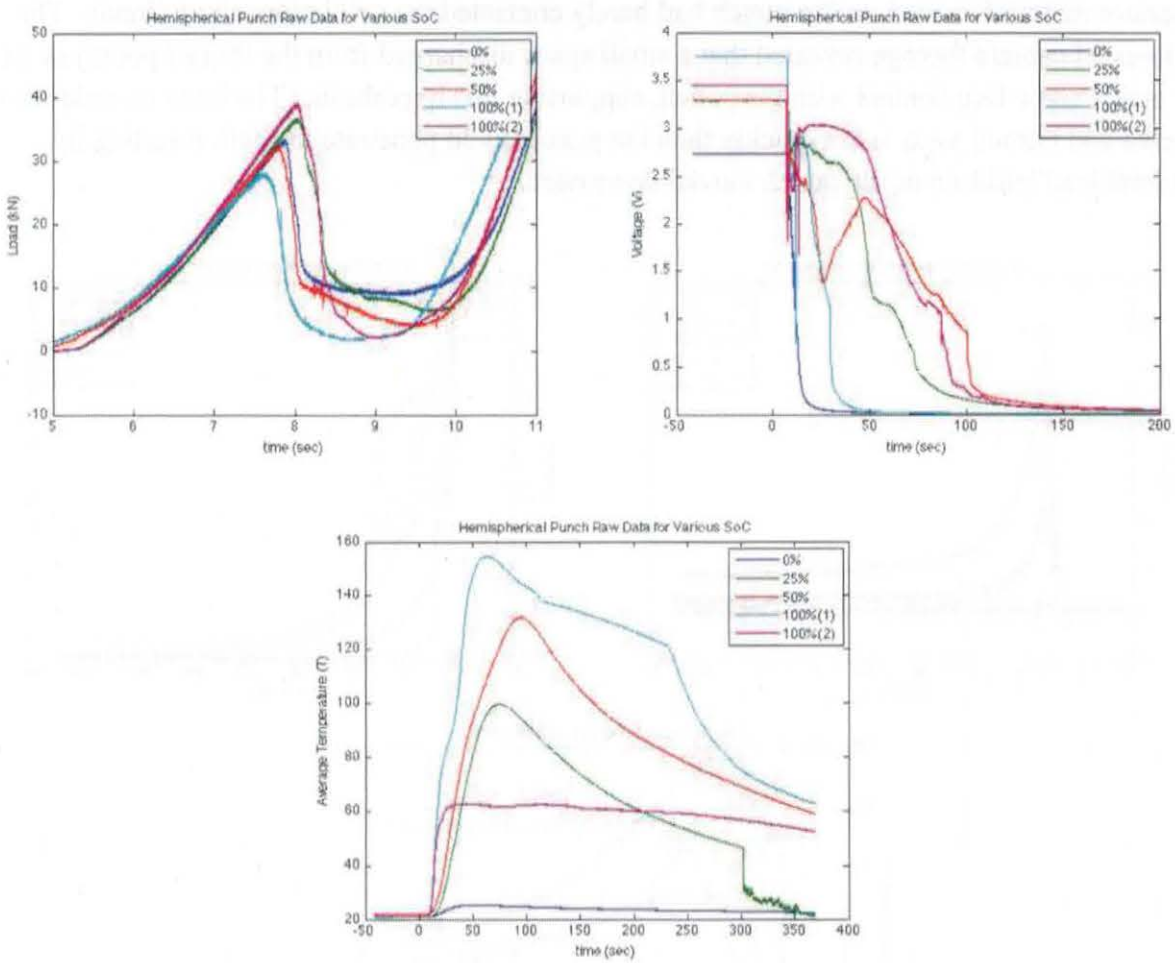

Figure 21: Plots of load, voltage, and average surface temperature vs. time for hemispherical punch tests.

Conical Punch Tests

Figure 22 gives plots of load, voltage, and surface temperature versus time for tests using the conical punch at various states of charge. The conical punch tests differed slightly from the hemispherical tests in that a thick sheet of Plexiglas was placed beneath the test cell, and hydraulic pressure to the ram was stopped once the punch contacted the Plexiglas surface. This was done to prevent damage to the punch, which could distort test results. Otherwise, the tests were performed in the same manner as the hemispherical punch tests.

Like the hemispherical tests, no clear pattern or progression of results were noted, not even with regards to the peak cell surface temperature or rate of increase. Note in Figure 22 that the 25% and 50% SOC load results were almost identical. Evidence exists to show that the 100% SOC cell reacted prematurely, as the result shows essentially zero load build-up before reaction occurs, indicating that the conical punch likely indented the cell at a location where a flaw in the

separator material existed, as the punch had barely contacted the cell before short circuit. The high-speed camera footage revealed that a small spark discharged from the impact point just as the punch came into contact with the pouch, supporting this hypothesis. The layer material then reacted and burned away more quickly than the punch could penetrate the cell, resulting in minimal load build-up as the punch moved downward.

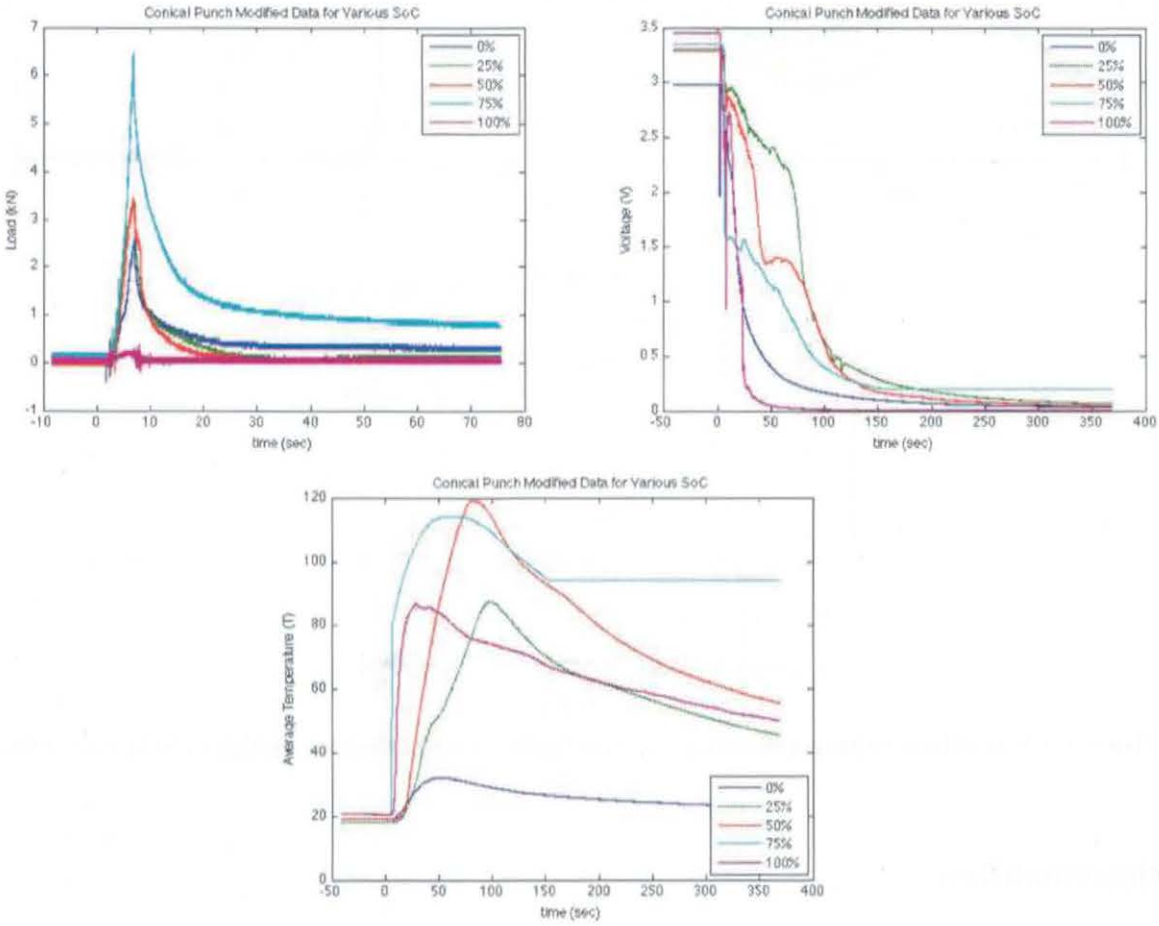

Figure 22: Plots of load, voltage, and average surface temperature vs. time for conical punch tests.

Of important note is an anomaly witnessed during the test of the 75% SOC cell. During this test, the conical punch penetrated the cell all the way through to the bottom with a peak load of about 6500 Newton. After stopping the ram, the cell failed to react or short circuit. The test team allowed the cell to sit for several minutes, yet no reaction occurred. The decision was made to "bump" the ram downward for a brief second to see if a reaction could be initiated. The cell finally did react, however the reason for the unusual behavior was never discovered. The delay in the reaction caused a gap in the data that made graphical comparison difficult, so the gap was removed from the data to allow for meaningful plot development. Figure 22 was corrected to eliminate the gap.

Flat Compression Tests

Previous testing with small [11] and medium-sized fully discharged prismatic pouch cells (Section 2.3) showed that when subjected to flat axial compression up to 200 kN, no short circuit of the cell occurred, however, the liquid electrolyte normally free flowing within the pouch and internal components was forced from between the layers, creating long blisters in the pouch around the edges of the anode and cathode layer stack. The purpose of these newer tests was to determine if the stack integrity would hold for cells subjected to loads up to 500 kN, and then to determine what effect, if any, the load and resulting electrolyte displacement had on the cell's charge capacity.

Following the 0% and 100% SOC flat compression tests, the cells were run through charge and discharge cycles to determine charge capacity. Neither cell exhibited any reduction in capacity as a result of the tests. The flat compression tests are not plotted because only load vs. displacement data would have been useful, and no changes in voltage or temperature were noted during the tests.

3.4 Observations and Conclusions

With the exception of the hemispherical test surface temperature, no trends or logical progressions were noted in the specimens as a function of SOC. Without repeating each test several (7 to 10) times, it is not possible to determine if the results observed are statistically significant or within normal cell scatter, or if the results are repeatable and to what extent so.

The reason for the failure of the 75% SOC conical punch test to short circuit remains to be understood, and may simply be a (highly unlikely) anomaly. Another postulate is that perhaps the separator material stretched as the punch penetrated the cell, and kept the layers from contacting one another until several minutes later when the punch was bumped downward.

Except for the small spark noted during the 100% SOC conical test just as the punch penetrated the pouch, the high-speed video footage did not provide any visual insight into the reactions that could not be seen on the regular footage.

The reaction (thermal runaway) of the cells, particularly at SOCs above 25% results in the rapid vaporization of the cell electrolyte and rupture of the pouch along an edge seam. The vapor is highly flammable, poisonous, and exits the pouch at temperatures as high as 150°C above ambient. Without the ventilation and exhaust system running, the team would not have been able to see the cell undergoing the reaction due to dense vapor filling the enclosure, and follow-on testing would have been severely delayed waiting for the vapor to dissipate before opening the enclosure for cell removal and cleaning.

As mentioned in Section 3.3 of this thesis, the use of surface temperature is likely a poor method of measuring the rate of thermal runaway. As the reaction occurs within the cell, the electrolyte vaporization resulting from temperature rise causes the pouch to inflate, creating an insulating vapor layer between the surface thermocouples and the active cell layers, where the reaction is taking place. A better method of temperature measurement might be to prepare special test cells with internal thermocouples to obtain more accurate and representative data. A related observation is that a more concrete definition for "thermal runaway" and a globally accepted method for measuring it should be established. It is possible that a measure of the amount and/or rate of electrolyte vapor produced might play a role, however parameters like this are very difficult to measure.

The method of initiating the reaction event is not optimized. The use of a hydraulic cylinder does not allow precise control of the punch, and precludes analysis of parameters such as punch penetration depth and material strain rate. If a standard test machine such as the one used to complete discharged cell testing in Section 2.0 could be fitted with the armored enclosure used for this testing, it is possible that test plans could be developed that would yield results from which more conclusions could be drawn.

Table 4 summarizes the test results in terms of observed cell reaction for the testing. From the results, it can be concluded that the level of thermal runaway a cell exhibits is proportional to the state of charge, with the exception of the flat compression tests, to which the cells appear extremely tolerant. Recall that two cells were tested with the hemispherical punch on 100% SOC cells in a failed attempt to prove repeatability of results.

% SOC	Hemi Punch	Conical Punch	Flat Compression
0	No Reaction	No Reaction	No Reaction
25	Minimal Reaction	Minimal Reaction	
50	Some Reaction	Some Reaction	
75		Large Reaction (Delayed)	
100	Largest Reaction (1) & (2)	Largest Reaction	No Reaction

Table 4: Charged cell test result summary.

4.0 Uniaxial Tension Tests of Cell Components for Material Characterization.

4.1 Introduction

When modeling objects with FEM software such as LSDyna, the object being modeled must be assigned material properties. Most FEM software packages include an extensive library of common and even uncommon materials that the user can choose from, including various metal alloys, wood species, and the list goes on. If a particular material of interest is not included in such a library, the programmer can create a user-defined material if the desired properties are known or select a suitable material that exhibits similar behaviors to the material being modeled.

Until this year, lithium-ion battery cell research performed by the MIT ICL had primarily involved calibration and refinement of homogeneous finite element computer models which were tested and validated with compression loading, but more precise behavior prediction can be obtained if the homogeneous block is refined by inputting details of tensile behavior of the multi-layer and multi-material system. Additionally, having properties of each layer would help to develop multi-scale models for the system, where locally we will have detailed model of all layers, and can study sequence of deformation and failure, while globally we will have the homogenized elements and their interactions with the battery pack casing and surrounding environment. The homogeneous FEM developed by Sahraei et al [8] utilized crushable foam properties from the LSDyna library to model the cell material with good results, but more detailed modeling will require separate materials to be identified for each component.

The component materials to be tested had thicknesses between .009 and 0.200 millimeters, which meant performing tests would not be a trivial exercise due to their delicate nature. So, in this final phase of the author's research, processes were developed to obtain repeatable results and prevent specimen damage. Collection of property data for cell components to support accurate selection of FEM properties was the ultimate goal of this effort.

Research in this area is ongoing, and a multilayer FEM was not completed prior to publication of this thesis. Since conclusions are not available on the performance of such models, this section will report only on the research planning, techniques, and preliminary data obtained from the material characterization tests conducted. Only component testing of materials of like chemistry to the small cells described in Section 1.4 were tested in this study. Future research will include testing on large and possibly medium size cell components.

4.2 Equipment Description

Several pieces of equipment were purchased to conduct component testing at the Impact and Crashworthiness Lab. Major equipment used for the research is described in this section.

Instron Test Machine

The primary instrument used for obtaining load versus displacement data was an Instron Test Machine Model 5944, fitted with a 100N load cell and a pair of 2 kN pneumatic grips. The computer controlled stand utilized Instron's Bluehill®3 software package. The grips were fitted with 25x32mm rubber grip faces, selected for their ability to grip the specimen faces without slipping. The stand and control station were sized such that both fit on a desk-sized footprint as shown in Figure 23. Maximum loads from the tests would not exceed about 30 N, so a 100 N load cell was selected for data collection since it was the smallest cell available for the load ranges expected and would produce very precise load measurements.

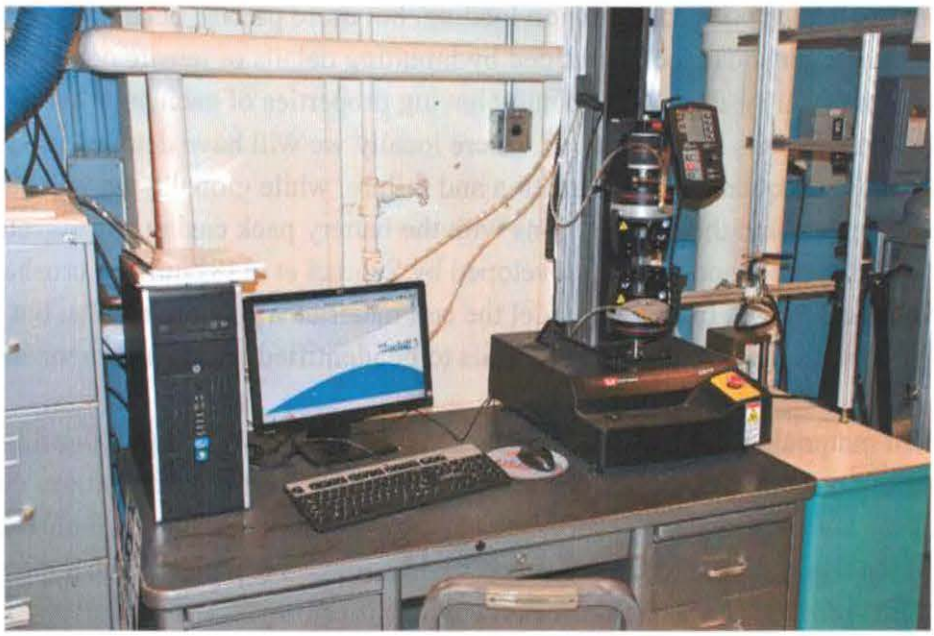

Figure 23: Test stand and control station for uniaxial tension tests.

Specimen Templates

To conduct the required uniaxial tension tests and obtain useful data, dogbone specimens of the component layer materials were required. Three templates were cut from thin aluminum on a water jet cutting machine. The templates were sized to conform to dogbone specimen requirements of ISO 6892-1 [18] to the maximum extent possible. It should be noted that the Standard provides requirements for specimens as thin as 0.1 mm, but many of the specimens tested were thinner than this.

The three templates were made with parallel lengths (Lp) of zero, five, and ten millimeters, with transition curves of 20-millimeter radius. Figure 24 illustrates the dimensions for the template with Lp = 10 mm used for final data gathering (left), and the cutting implements with all three templates (right). The other two templates were identical in overall size; the only difference was that the centers of the radii were modified to get parallel lengths of zero and five millimeters. The Lp = 0 mm and Lp = 5 mm templates were tested, ultimately the Lp = 10 mm template made the best specimens. The overall dimensions of the specimens were chosen so they would be of similar scale to biaxial testing slated for future work.

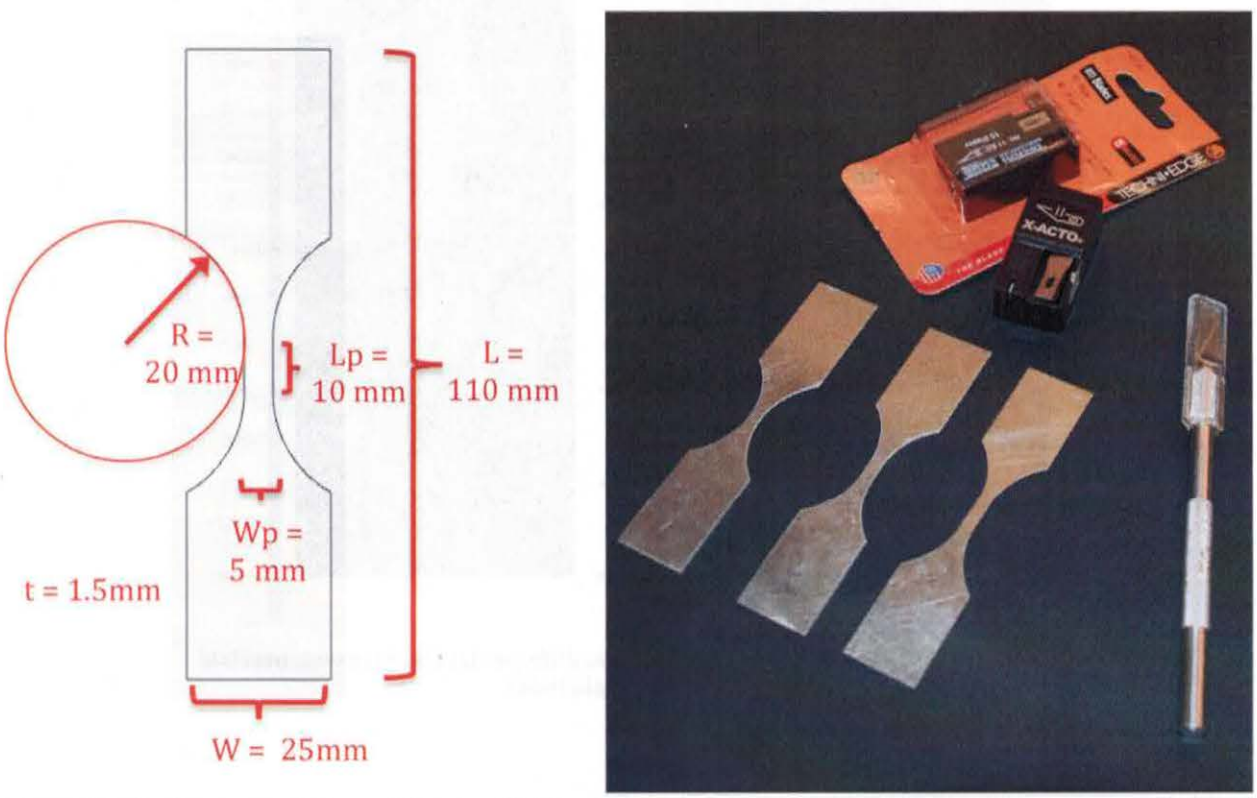

Figure 24: Specimen template specifications (left) and three manufactured templates with cutting tools (right).

Digital Image Correlation System

To obtain highly accurate strain information for each specimen, a digital image correlation (DIC) software package was employed. Developed by Correlated Solutions, the package consisted of Vic-Snap® software which controlled exposure levels and image capture frequency from a Q-Imaging Retiga 1300i digital camera, and Vic-2D® software which calculates the strains. Vic-2D® tracks dot displacement on a specimen surface as it is placed under tension or compression. Following a complete displacement analysis of a properly prepared specimen, Vic-2D® can very accurately determine strain at any point within an area of interest on the specimen surface. Figure 25 shows two images of a lithium-ion battery separator specimen with DIC processing

applied to show strain in the vertical direction (ε_{yy}). The left image has a lower applied load than the right. If accurate strain data can be obtained in both the machine and transverse directions of a specimen, then useful material properties such as Poisson's Ratio can be calculated for use in finite element modeling.

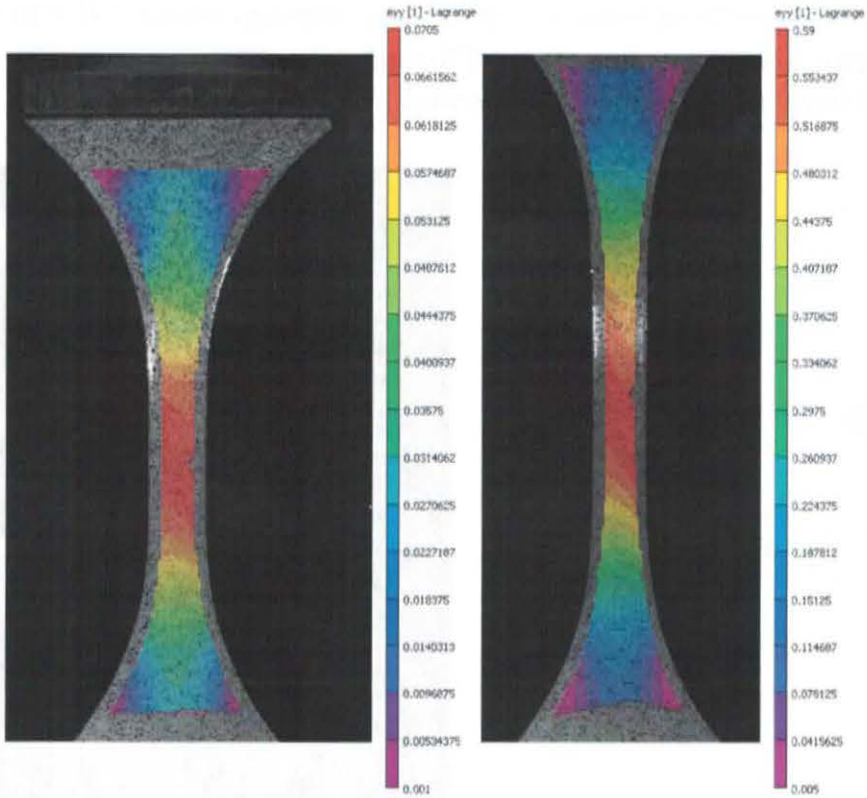

Figure 25: Cell separator specimen at two different levels of tension, overlaid with DIC strain fields.

4.3 Test Material Description

Dry, electrolyte-free sheets of cell layer materials with coatings of the same chemistry as the small cells used in earlier material characterization tests were obtained from a scientific research supplier. Rolls of uncoated, plain aluminum and copper foils of the type used to construct the coated anode and cathodes were also obtained. Toxicity and corrosiveness of the electrolyte in fully assembled cells precluded the possibility of testing "wetted" layer materials in our laboratory.

Data collection began by first obtaining load versus displacement data for specimens of the plain copper and aluminum foils. Uniaxial tension testing of dogbone specimens cut in both the machine direction (MD) and transverse direction (TD) was completed to determine if any differences existed in material behavior, such as anisotropic properties. Once plain foil testing was complete, coated anode and cathode specimens were tested in the same manner. The

purpose of completing plain foil and coated foil tests was to determine what effects the coating alone had on the layer properties, as it was not possible to separate the coating from the foil for testing. Finally, tests were performed on similarly prepared separator material specimens.

During the plain foil tests, separate tests of paint speckled and non-speckled specimens were tested to determine if a fine mist of paint, needed for accurate DIC measurements, would affect test results. The data showed that a very fine mist of flat black spray paint in which individual speckles did not connect into large spatters had no effect on the test results. In contrast, the use of paint speckling did not produce good results on coated specimens. Details of attempts to obtain good strain results for coated specimens are provided in Section 4.6 below.

Anode Layer

The anode layer consisted of a thin copper foil of thickness .009 mm, coated on both sides with CMS graphite for a total thickness of 0.100 mm, meaning the thickness of the coating on each side is approximately 0.045 mm thick.

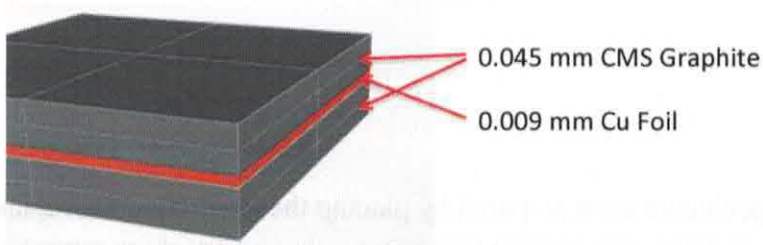

Figure 26: Conceptual drawing of anode layer.

Cathode Layer

The cathode layer consisted of a thin aluminum foil of thickness .015 mm, coated on both sides with Lithium Cobalt Oxide for a total thickness of 0.200 mm, meaning the thickness of the coating on each side is approximately 0.0925 mm thick.

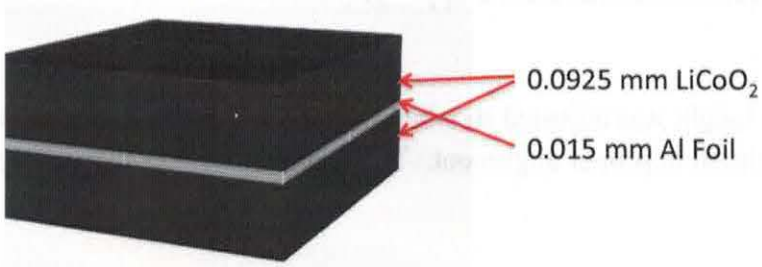

Figure 27: Conceptual drawing of cathode layer.

Separator Layer

The separator layer consists of a material called Celgard®, which is rolled and then stretched, causing it to separate and create small pores through which the electrolyte can pass, but contact between anode and cathode layers in a cell is prevented. This material drawing process is called "crazing". The finished thickness of the separator material is only 25 microns. Figure 28 shows a layer of separator material captured at high magnification using an electron microscope.

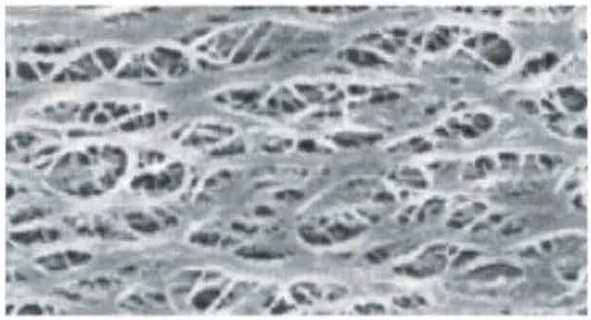

Figure 28: Typical cell separator material at high magnification, courtesy MIT ICL.

4.4 Test Setup

Component layer specimens were prepared by placing the Lp = 10 mm template on the sheets of layer material, then meticulously cutting the shapes using a very sharp razor knife. Blades were changed out frequently, at the first sign of becoming dull, as failure to do so would result in an unacceptable specimen edge, as described in Section 4.6.

The specimens were then very carefully attached to one of the upper grip faces removed from the test stand with a small piece of adhesive tape, all the while specimen handling was minimized. The specimens were so delicate that even light breeze from moving the specimens from the cutting table to the test stand could cause deformation. Once the specimen was attached to the grip face, the face was reinstalled into the upper grip assembly of the test stand and the grips were closed.

Next, the specimen height was adjusted so when the lower grip was closed, the faces would firmly grip the specimen in proper alignment. The load cell was balanced just prior to closing the lower grips.

4.5 Test Execution and Results

Anode and cathode specimens were drawn at a constant crosshead speed of 0.2 mm per minute (quasi-static), but the separator specimens required so much displacement to fail that the

crosshead speed had to be raised to 4.0 mm per minute, a factor of 20 times faster to prevent creating excessive photo data files. Load and displacement data was recorded at 0.2-second intervals, and DIC images were taken at one-second intervals for all materials. The load displacement data and DIC image files were synchronized using a stopwatch to facilitate their correlation during post-test processing.

Anode Layer

The copper foil MD and TD tests showed that the material was isotropic, so only MD tests were performed on the coated anode specimens. Figure 29 below shows a load versus displacement comparison of the plain foil samples (left) and the coated samples (right). Notice that in both cases, the failure is a gradual tearing of the specimen, and not instantaneous failure.

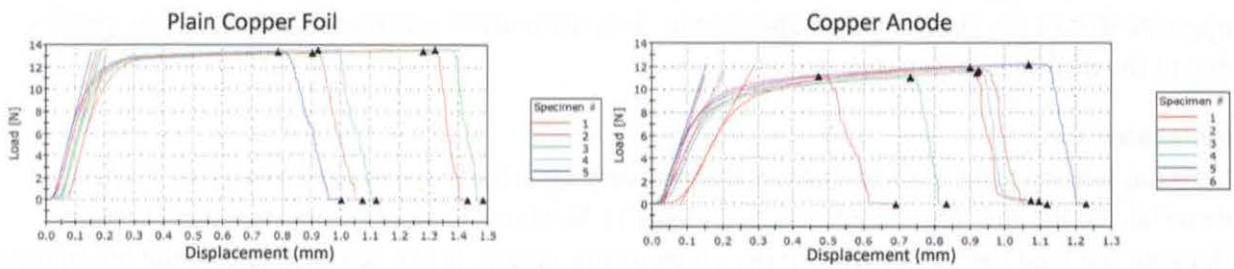

Figure 29: Comparison of plain copper foil to copper anode in uniaxial tension.

The results were processed and averaged to determine the mean difference between the coated and uncoated properties. Details of the results of that effort may be published in future works, but for the purposes of this thesis, the point to note is that the change in modulus between plain foils and coated specimens is a reduction from 22.25 to 17.48 MPa respectively. The change in slope can be seen from the plots despite the slight difference in x-axis scale. Also, it can be seen that in the plastic region, the plain copper load reaches about 13 N, and then remains about constant for a long period, whereas the coated samples make a more gradual climb to 12 N before failure.

Cathode Layer

Unlike the copper foil specimens, the aluminum foil demonstrated anisotropy between the MD and TD tests. Consequently, the coated cathode specimens were also tested in both directions. It should be noted that very fine lines from the rolling process were clearly visible in the aluminum foil samples, which were not noted on the copper foil. Figure 30 below shows a load versus displacement comparison of aluminum foil to cathode layer in the machine direction (MD). The differences between plain foils and coated cathodes in the transverse tests were similar, and not shown in this report. Note in the figure that unlike the copper foil/anode tests, the aluminum/cathode tests fail instantaneously and at a lower load and total displacement than the copper/anode specimens.

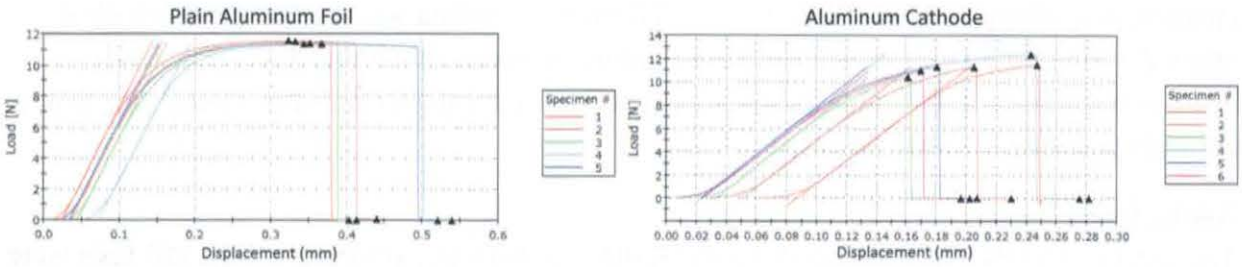

Figure 30: Comparison of plain aluminum foil to aluminum cathode in uniaxial tension.

Similar to the copper anode specimens, results were averaged and the mean differences between the two were calculated. An interesting note is that the change in mean modulus between plain foils and coated cathode is an increase from 12.78 MPa to 13.45 MPa respectively, a behavior opposite that of the copper/anode specimens. It is difficult to see this visually form the graphs due to the differences in x-axis scales.

Separator Layer

Uniaxial tension tests of the separator showed very significant anisotropic behavior of the material. In the MD tests, loads reached about 13 N, about 13 times more than the TD tests. Because the load rose so slowly for the given displacement, it was reasonable that the modulus is only about 0.02 MPa. The modulus for the TD samples is essentially zero. These results are not a surprise based on what is known about how the separator is made. By looking at Figure 28 in Section 4.3 we can see from the way the porosity of the material is formed that it will behave differently depending on the direction it is stretched. Figure 31 shows load versus displacement plots for the separator in the machine (left) and transverse (right) directions.

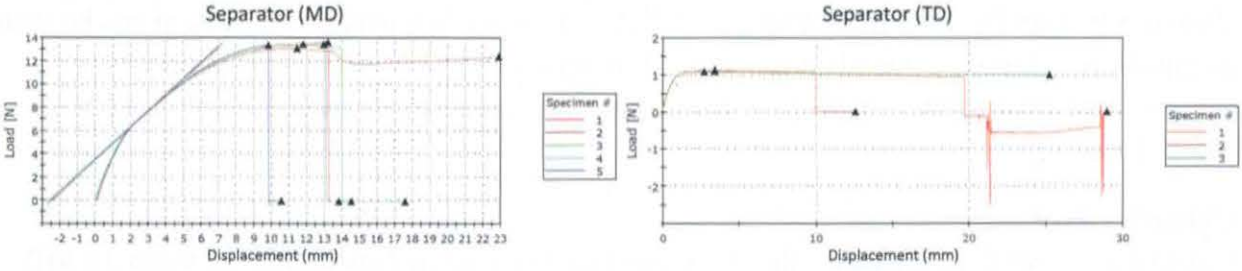

Figure 31: Comparison of separator layers in MD (left) and TD (right), uniaxial tension.

In both cases, a very large total crosshead displacement was required to obtain material failure. The material behaves completely different in the transverse direction than in the machine direction. It should be noted that large displacements like this are unlikely in battery abuse situations. The most likely cause of a separator failure would be high tension across a very small, local length (perhaps millimeters) caused by the intrusion of an object into a cell similar to tests conducted on Sections 2.0 and 3.0 of this thesis.

Four-Layer Tests

Following completion of the individual layer testing, four-layer sandwich specimens were tested. The four layers represent the smallest repeatable unit of the within a battery cell, and data obtained from these tests may prove useful for defining properties for an upcoming iteration of the FEM design in which the four repeating layers together make up the smallest model unit.

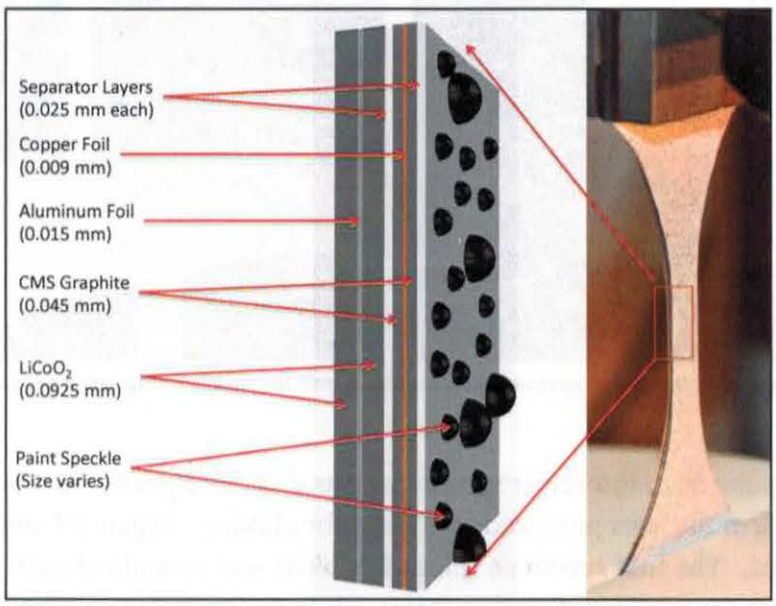

Figure 32: Conceptual drawing of four-layer test specimen with light paint speckling for DIC (left) and actual specimen installed in fixture for testing (right).

The layers were arranged in separator-anode-separator-cathode order, carefully stacked and joined at one end only with a very thin, double-sided adhesive tape. Figure 32 depicts a magnified view of the specimen layers represented by the small red rectangle in the image to the right. The top layer of separator was lightly speckled with flat black paint for DIC tracking.

The assembly was placed into the test machine in similar fashion to other specimens, however in order to eliminate buckles and gaps and to ensure the grips exerted equal tension to all layers, they needed to be held together by a lightweight fixture. After closing the upper grips, the specimen stack was compressed between two business cards as the lower grips were closed. The cards were then folded down to expose the specimen to the DIC camera. Attaching the layers at only one end permitted free movement or sliding relative to one another so the stack would lay flat during installation into the grips. Figure 33 shows a photo of the layer stack compressed with the business cards (left) and then a photo of the flat layer stack ready for testing with the cards folded down and secured.

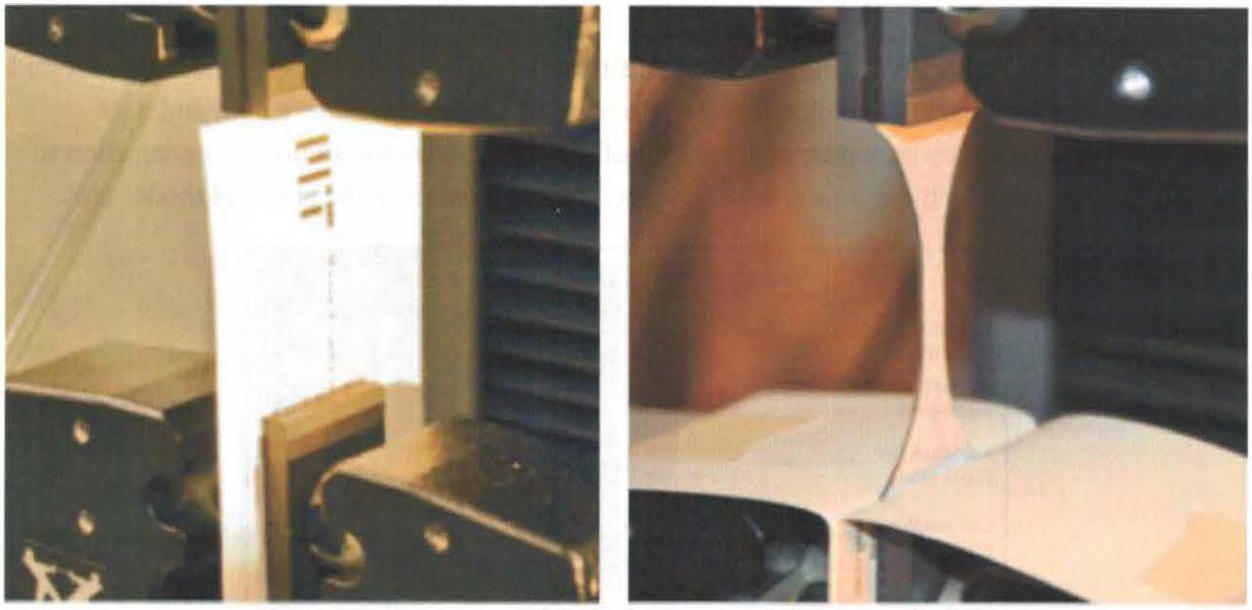

Figure 33: Four layer specimen installation into test grips using business cards.

Obtaining good results from four-layer specimens was difficult at best. Several tests were run, but only about 50% of the tests produced good data for plotting. Figure 34 shows typical results from two specimens. The first specimen (plotted in blue) was assembled such that each layer would see tension in the machine direction (MD), while the second specimen (plotted in red) was assembled such that all layers would see tension in the transverse direction (TD).

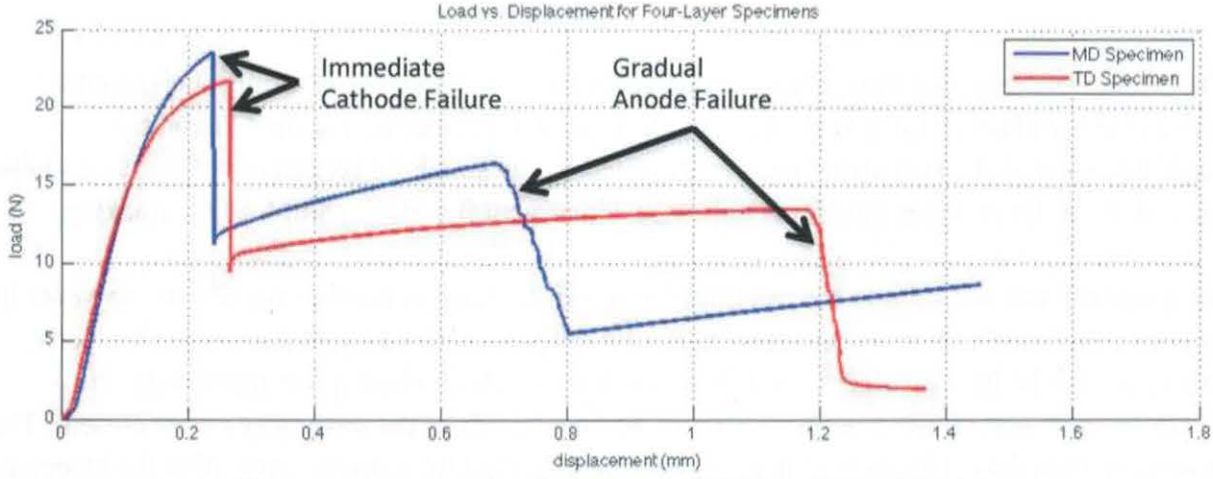

Figure 34: Typical results of four-layer specimens in uniaxial tension.

It can be shown that testing the four-layer specimens gives similar results to the summing of individual test data. Consider only the MD specimen of Figure 34 given by the blue line. From zero to about 0.24 mm displacement, the load curve is the sum of the tension of the four components, and then the aluminum cathode layer fails, so a sharp drop in load occurs. From

about 0.24 mm 0.7 mm, the load curve is a summation of only the copper anode and two layers of separator until the copper gradually fails. From 0.8 mm on, we see the gradual rise in load from only the two layers of separator material. Note how this differs from the TD specimen plotted as the green curve, where following the failure of the copper anode, the load simply falls towards zero because the separator in the transverse direction has no strength. Because the separator may not fail until displacements in excess of 10 mm are reached, the tests were stopped prior to separator failure.

The following analysis demonstrates that the four-layer tests are essentially a summation of individual tests. Three specimens were selected from the results illustrated in Figures 29, 30, and 31 above:

- Copper Anode Specimen #3
- Aluminum Anode Specimen #1
- Separator Specimen #5

All three specimens were tested in the machine direction (MD), and are plotted on a common set of axes in Figure 35.

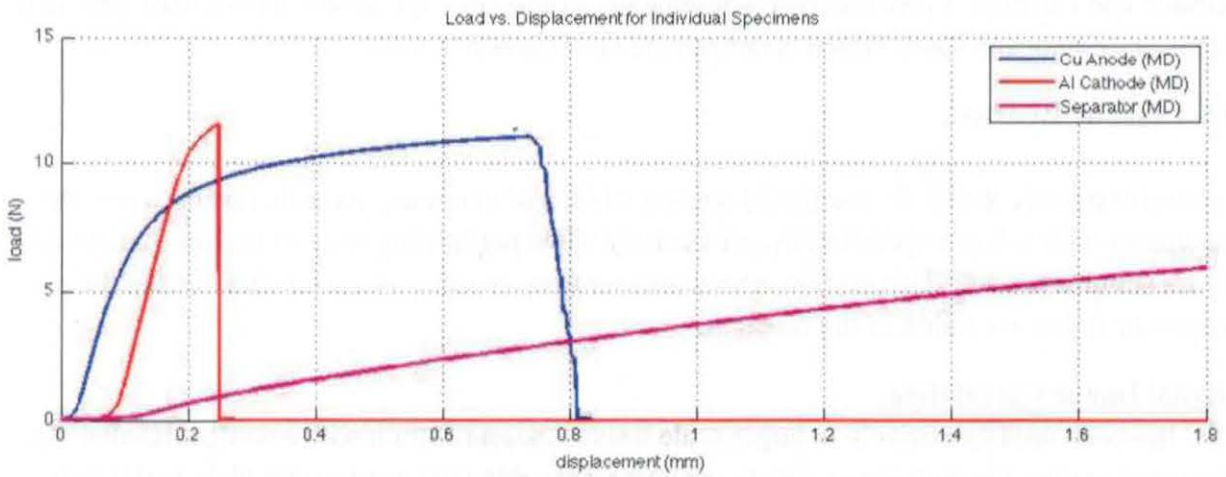

Figure 35: Plots of individual component layers used to model four-layer specimen test results.

By summing the load values of the components for the given values of displacement, a plot similar to that shown in Figure 34 can be produced. Figure 36 shows the original four-layer MD result plot again as a blue line, and compares it to the component summation plotted in magenta. The two results are remarkably similar.

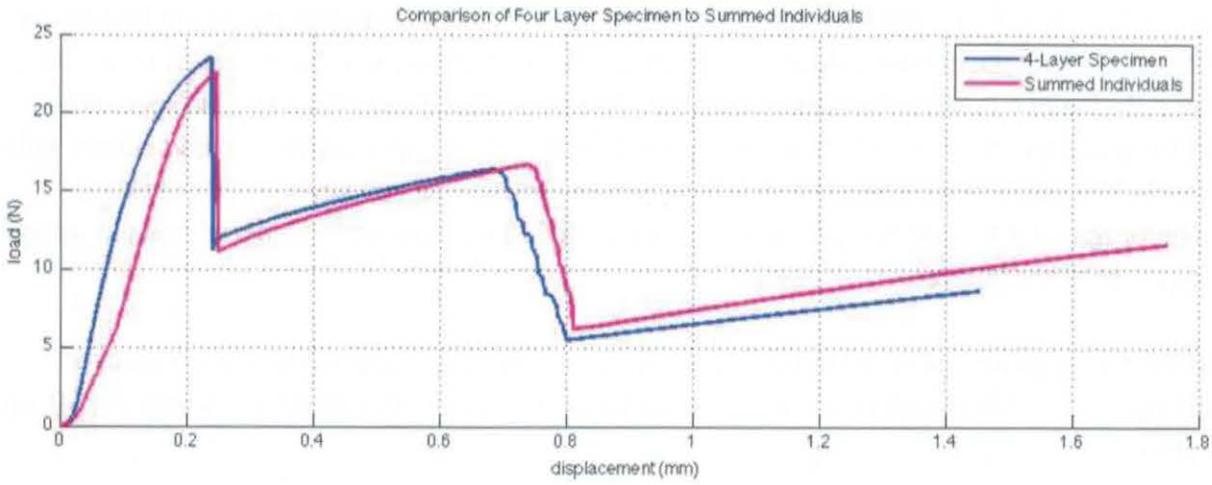

Figure 36: Comparison of four-layer specimen result (blue) to summed individual layer result (magenta).

Note that the separator curve is added twice since there are two separator layers in a four-layer specimen. The author admits that individual specimens were selected for comparison for their similar characteristics to the results in the four-layer plot, but they were selected only for their behaviors relative to the displacement, not load. As an example, the anode specimen chosen was one that failed near the 0.8 mm displacement point, as seen in the four-layer test. No consideration was given to the peak load of the specimen(s). The only way to really prove the relation and calculate a percent-error would be to test the same specimens individually and then again as a composite stack, which is not possible in destructive tests!

4.6 Lessons Learned

Testing extremely thin foils in uniaxial tension while still obtaining accurate results is possible but comes with a degree of difficulty, particularly when performing tests on multiple component layers simultaneously. This section attempts to summarize some of the hurdles that had to be overcome in the execution of the research.

Digital Image Correlation

DIC has been used extensively in larger scale tests to measure strain with excellent results. As discussed earlier, the author was able to achieve reasonable DIC results with plain metal foils and separator material by the application of very fine paint mists to the specimen surface. Evaluating coated samples proved much more difficult. The coated specimens are usually a darker color by nature, so a very fine mist of white spray paint was applied to create the contrasting dot pattern used for DIC. The paint did not tend to bead up into small dots on the coating surface as desired, rather it tended to absorb into the coating, leaving a pattern resembling thin clouds which was not easy for the DIC software to track. Additionally, the coating consists of fine granules of material, some of which reflect light. The light used for obtaining DIC images tended to reflect back into the camera at least part of the time during a test, which the software would mistake for white dots. As the specimen would stretch under

tension, many of the reflected particles would move such that they were no longer reflecting the light, and the software would become further confused.

The author attempted to apply a thin coat of flat black paint to the surface before the application of white paint to eliminate reflection problems, but under a microscope it could be observed that the coating was actively absorbing the black paint. This means that the paint is likely changing the properties of the coating – either the solvent in the paint carrier is breaking down the binder, or the paint is reducing the resilience of the coating as it dries. Either way, it is not possible to obtain accurate properties of the coating when it has been contaminated by paint.

Specimen Cutting

Finding a method of cutting the sample material such that the specimens are uniformly sized and have clean edges was also a significant challenge. Using a punch-type cutter will not produce a clean edge, nor will a pair of precision scissors due to the extremely fine thickness of the material. The author eventually chose to use a thin aluminum template and razor-knife method due to ease of use and reasonable results, but great care must be taken to prevent damaging the template with the knife while cutting samples, which would alter the final dimensions of the future specimens cut.

When making straight cuts, the knife produces a reasonably smooth edge if the material is placed on a hard surface with one or two sheets of plain white office paper placed underneath. The result is not as clean when cutting along a curve, as the material tends to tear rather than cut. This is particularly true for the aluminum materials. The problem of the curved-cut tearing can be overcome by employing templates with a non-zero parallel length. This is one of the reasons the template ultimately selected for testing had a parallel length of 10 mm. Figure 37 shows 50X-magnified views of the aluminum foil material with straight (left) and curved (right) cuts for comparison.

An interesting paper was written by Huh et al [19] on the precise cutting of very small specimens for MEMS research in which he cut dogbone specimens using a micro-photo etching process. The ICL has asked, and Dr. Huh has agreed to attempt to cut samples of our layer materials using his process, but those results were not complete at the time this thesis was published. Early reports were that the plain foil samples were possible, but the chemicals used in the photo etching process tend to soak into the coating on anode and cathode specimens, hampering success with those materials.

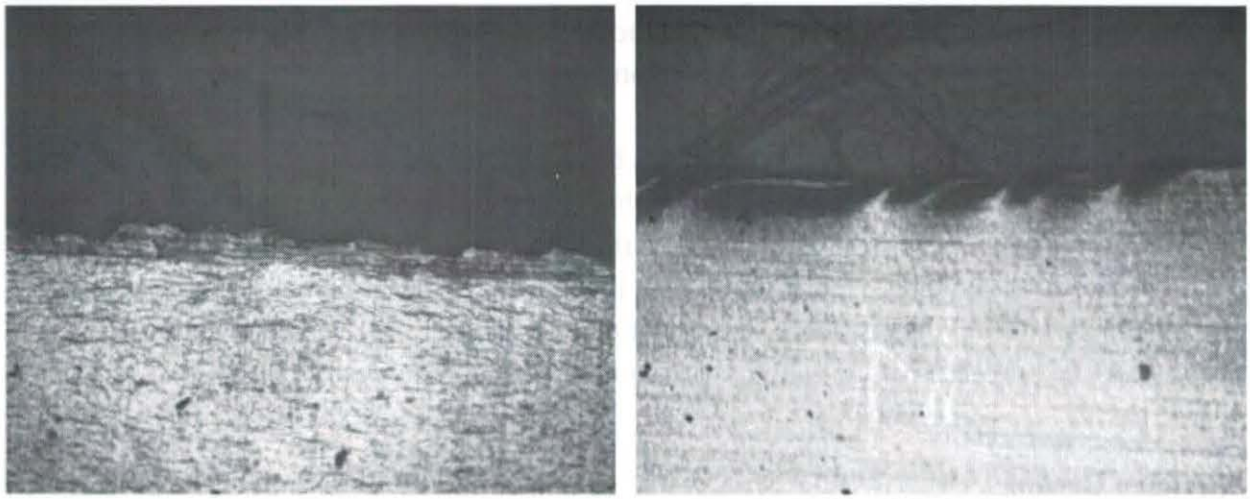

Figure 37: High magnification view of specimen edge for (L to R) straight and curved cuts.

Eccentricity of Test Stand Grips

The small scale of the test specimens posed an additional problem in that there is some eccentricity, or misalignment of the grips that could be affecting the precision of the test results. Figure 38 illustrates the degree of the problem. The rubber grip faces shown are 32 mm in length for reference, with the resulting axial offset being between 1-2 mm.

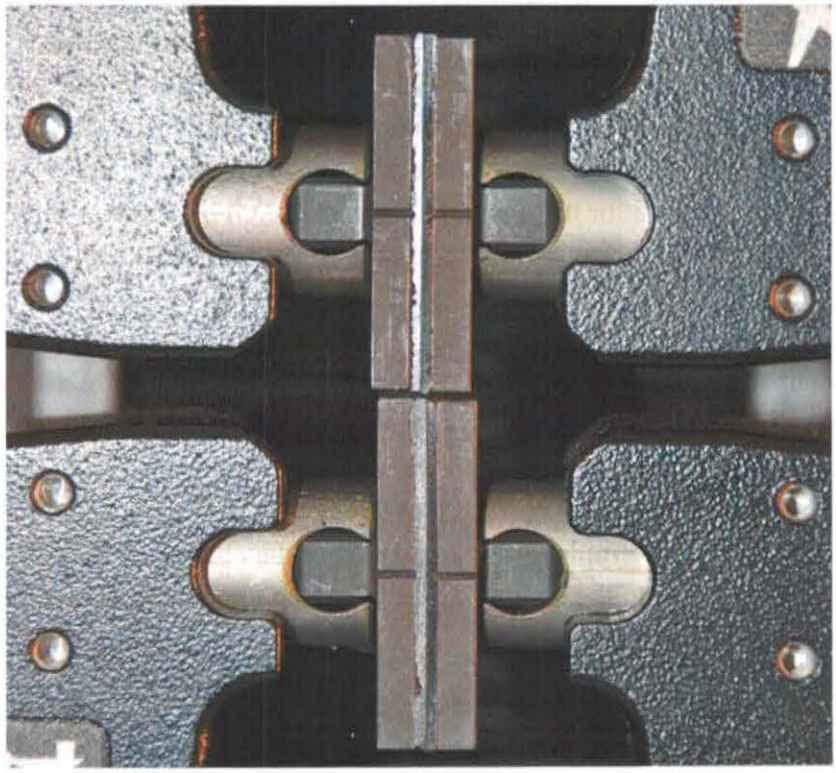

Figure 38: Illustration of grip misalignment.

While the eccentricity appears minor in the photo, when the scale of the specimens is considered, this degree of misalignment is significant. For future work, a special fixture should be produced with alignment pins that eliminate the problem, so specimens are subject only to pure tension.

Paint Speckling for DIC

Performing DIC on test specimens using high contrast speckling on the material surface has revolutionized the way strain is measured in industry. All that is needed is a suitable surface to apply the speckling and the ability to capture timed images for computer tracking of the dots. Surface speckling is typically accomplished by applying a fine mist of spray paint to a clean surface. If the surface is light colored such as aluminum, then flat black dots are applied. For darker surfaces, flat white dots are applied. If the surface tends to reflect light, then a complete coating of either color flat paint followed by a speckling of the opposite color will eliminate reflection issues.

While good results were obtained when flat black speckling was applied to plain foil and separator samples, similar success was not enjoyed with the coated samples. Several factors caused DIC of the coated samples to be problematic. Major problems are outlined below:

- The plain foil and cathode samples are extremely thin. It is important that if any speckling is applied, the adverse effects of data skew or increased sample thickness are minimized and/or accounted for.
- The coating tends to reflect light, which confuses the DIC software because the reflections appear to be small white dots, which can appear and disappear. Eliminating the reflection problems would require a full base layer coating of paint, violating the first point above.
- When paint is applied to the coating surface, the coating absorbs the paint, leaving a cloudy residue on the surface rather than clean round dots, which reduces the accuracy of the software's displacement and strain calculations.
- The paint is carried from the can to the surface via a solvent. The effects of the solvent on the binder material that holds the active coating on to the foil is unknown, therefore making it difficult to draw any conclusions about the coating properties from test results where paint is used.

At the time of this writing, only preliminary processing of strain data was completed for plain and coated foils. The results thus far for coated specimens have not produced strain data clean enough to accurately refine some material properties, such as Poisson's Ratio, due in part to noise in the data. Much of the noise appears to be at the beginning of the test runs, but coating reflectivity problems described earlier also produce noise throughout the tests. Only further data smoothing will show if accurate strain data by DIC is possible for coated specimens. Until a solution is found, the team is limited to the use of classic methods of obtaining engineering strains from test machine crosshead displacement.

4.7 Conclusions and Recommendations

While the purpose of this research (further refinement of the battery cell FEM) is not complete, the data obtained from the testing plan will serve that end, and the methods for specimen preparation and handling developed can be used to conduct additional testing for other battery cell types in the future. Results of FEM refinement will be reported in the common literature at a later date.

When test results of plain foils are compared to coated samples, a significant change in modulus is noted. The change is opposite between the anode and cathode layers.

A detailed analysis of the in-line and transverse strains from coated specimens is still in progress. Preliminary results show that the coatings do not tend to behave in the same manner as the underlying metallic foil. Further analysis is needed to eliminate possible noise at the beginning of test runs before final conclusions can be drawn.

As of the writing of this report, a reliable method to apply speckling to coated samples without risk of altering the coating properties and eliminating reflectivity issues has not been found. A solution is necessary to obtain accurate strain data from test specimens using DIC.

Four-layer specimen preparation and installation into the test machine is a difficult process. While these specimens give interesting graphical results, it might be concluded that going through such a difficult process to obtain data is not needed, as it can be shown that very similar results are obtained by summing the results of individual component tests, which are easier to conduct and show a higher incidence for producing useful data.

It should again be noted that all of the testing in Section 4.0 was performed on dry component samples. A method of accounting for this disparity from real-life battery cell conditions is needed.

5.0 Thesis Conclusions and Recommendations for Future Work

Conclusions

For many years now there has been an exponential increase in the energy density and compactness of lithium battery cells resulting from an incredible amount of research with that aim. As this technology becomes more and more common in everyday consumer products, particularly vehicles, it becomes increasingly important that the behavior of the cells under abuse conditions is thoroughly understood and ways to mitigate the danger are fully explored.

The research conducted for this thesis was an effort to enhance the current level of knowledge on the results of abuse testing and provide data for refinement of finite element models, which could be used to evaluate new and existing cell designs for safety.

In Section 2.0, additional research on the results of indentation of prismatic pouch cells was used to refine and validate homogeneous cell computer models. A rough linear progression was noted in the degree of indentation that cells can endure as a function of indenter size and shape to the point where flat compression of cells resulted in no damage.

Section 3.0 reports on exploratory research into the behavior of full or partially charged large prismatic pouch cells following indentation. The results showed that as the percent state of charge increases, so does the rate at which thermal runaway of the cell occurs. The thermal runaway of the cell results in a rise in the internal cell temperature, which, if high enough can result in vaporization of cell electrolyte and cell rupture.

In an effort to create a multi-scale finite element model for lithium-ion batteries, material characterization of cell components was conducted as described in Section 4.0. While the results of the tests are simply material property data, the difficulties in preparation and handling of the specimens to be tested were very interesting, as were the change in behavior of the layers as a result of the addition of coating.

Research into the effects of abuse on energy-dense products like lithium-ion cells tends to cast a negative light on the technology, and public release of such research is often discouraged by manufacturers; however, if one accepts the fact that a product is dangerous and develops effective measures to mitigate the risks, the product can still be used safely. Gasoline and natural gas are perfect examples; both products are toxic and highly flammable, but are commonly used every day by a majority of mankind.

Future Work

Lithium-ion battery research at the MIT ICL will continue for years to come. Currently in progress are material characterization tests similar to those outlined in Section 4.0 for large prismatic pouch cells. An effort to design and build a biaxial punch test fixture that allows for the use of three-dimensional DIC is also ongoing.

The following additional areas of study are suggested to enhance current research:

- Punch indentation of individual component layers atop dense crushable foam may produce component failure that is easy to inspect following the tests. This type of research may provide insight into mode of failure within complete cells.
- Further research into the behavior of the coating powder and binder is needed, to include an understanding of what effect the application of coating has on the strength of the foils.
- A partnership with a cell manufacturer should be established such that the manufacturer would produce special cells designed for abuse testing. These special cells might include internally embedded thermocouples to allow for more accurate temperature measurement, and development of a non-toxic electrolyte substitute that would permit post-testing dissection of the cells without the need for personal protective equipment or glove bags.

References

1. Commander, Naval Ordinance Center. "Technical Manual for Navy Lithium Battery Safety Program Responsibilities and Procedures." Naval Sea Systems Command, 2010.

2. Goldman, David. "U.S. Cell Phones, Tablets Outnumber Americans." *CNNMoney Tech*. New York, October 12, 2011, 2011 Oct 12 edition.

3. Consumer Product Safety Commission. *CPSC, Apple Announce Recall of iBook and PowerBook Computer Batteries* Recall Notice. Washington, D.C.: CPSC, May 20, 2005.

4. Consumer Product Safety Commission. *HP Expands Recall of Notebook Computer Batteries Due to Fire Hazard* Recall Notice. Washington, D.C.: CPSC, May 27, 2011.

5. Burden, Melissa. "GM Lab Damage Might Hit $5M." *The Detroit News*, April 20, 2012.

6. Smith, B. *Chevrolet Volt Battery Incident Overview Report*. NHTSA NVS-224, January 20, 2012.

7. Hill, Richard. "Development of a Representative Volume Element of Lithium-Ion Batteries for Thermo-Mechanical Integrity." Massachusetts Institute of Technology, 2011.

8. Sahraei, Elham, Richard Hill, and Tomasz Wierzbicki. "Homogenized constitutive model of the cylindrical lithium-ion battery cell." *Journal of Power Sources* no. 2010 (2010).

9. Sahraei Esfahani, Elham, Richard Hill, and Tomasz Wierzbicki. "Calibration and Finite Element Simulation of Pouch Lithium-Ion Batteries for Mechanical Integrity." *Journal of Power Sources* no. 2011 Nov (November 2011).

10. Wierzbicki, T, Elham Sahraei, and Richard Hill. "Li-Ion Cells with Experimental Validation." s.l.: *Journal of Power Sources,* 2011.

11. Campbell, John. "Development of a Constitutive Model Defining the Point of Short Circuit Within Lithium-Ion Battery Cells." Massachusetts Institute of Technology, 2012.

12. Sahraei Esfahani, Elham, John Campbell, and Tomasz Wierzbicki. "Modeling and Short Circuit Detection of 18650 Li-ion Cells Under Mechanical Abuse Conditions." *Journal of Power Sources* 220 (December 2012).

13. Wierzbicki, Tomasz, and Elham Sahraei Esfahani. "Calibration of the Mechanical Properties of the Jellyroll from Crush Tests on Cylindrical Li-ion Cells." *(Submitted to) Journal of Power Sources* (2012).

14. Sahraei Esfahani, Elham, Joseph Meier, and Tomasz Wierzbicki. "Characterizing Mechanical Properties and Onset of Short Circuit for Three Sizes of Li-ion Pouch Cells." *(Submitted to) Journal of Power Sources* (2013).

15. Pasztor, Andy, and Jon Ostrower. "Probe of Boeing 787 Battery Fire Expands." *The Wall Street Journal*, January 20, 2013, 2013 Jan 20 edition, sec. Business.

16. Greve, Lars, and C. Fehrenbach. "Mechanical Testing and Macro-mechanical Finite Element Simulation of the Deformation, Fracture, and Short-circuit Initiation of Cylindrical Lithium Ion Battery Cells." *Journal of Power Sources* 214 (September 15, 2012): 377–385.

17. Meier, Joseph D., Elham Sahraei Esfahani, Manfred Salk, Thomas Kisters, and Frank Huberth. "State of Charge Vs. Thermal Runaway for Lithium Ion Large Pouch Cells." *Battery Congress 2013* 1, no. 2013 (April 2013).

18. International Organization for Standardization. "International Standard ISO 6892-1, Metallic Materials - Tensile Testing." IHS Switzerland, 2009.

19. Kwon, J.B., J. Huh, H. Huh, and J.S. Kim. "Micro-Tensile Tests of Aluminum Thin Foil with the Variation of Strain Rate." *Dynamic Behavior of Materials, Springer, New York.* Conference Proceedings of the Society for Experimental Mechanics Series (2013): 89–100. doi:10.1007/978-1-4614-4238-7_12.